Energy & Buildings 338 (2025) 115713

Contents lists available at ScienceDirect

Energy & Buildings

journal homepage: www.elsevier.com/locate/enb

Prosumers and district heating: Experimental validation of strategies to improve thermal energy production and consumption

Paolo Sdringola [a,*], Mauro Pipiciello [b], Mattia Ricci [c], Federico Gianaroli [c], Diego Menegon [b], Federico Trentin [b], Francesco Turrin [b], Biagio Di Pietra [d]

[a] Energy Efficiency Department, Italian National Agency for New Technologies, Energy and Sustainable Economic Development (ENEA), Research Center Casaccia, Via Anguillarese 301, 00123 S.M. di Galeria, Rome, Italy

[b] Eurac Research, Institute for Renewable Energy, Viale Druso 1, 39100 Bolzano, Italy

[c] Energy Efficiency Department, Italian National Agency for New Technologies, Energy and Sustainable Economic Development (ENEA), Research Center Bologna, Via dei Mille 21, 40121 Bologna, Italy

[d] Energy Efficiency Department, Italian National Agency for New Technologies, Energy and Sustainable Economic Development (ENEA), Via Principe di Granatelli 24, 90141 Palermo, Italy

ARTICLE INFO

Keywords:
District heating
Prosumer
Self-consumption improvement
Heat pump integration
Bidirectional substation
Hardware-in-the-loop
Net metering

ABSTRACT

The European Union targets a 55 % reduction in greenhouse gas emissions by 2030 and climate neutrality by 2050, emphasizing decarbonisation in energy sectors. District Heating Networks with thermal prosumers and bidirectional substations are critical to decarbonize the heating sector by integrating renewable energy sources. The paper analyses how to enhance the share of renewable energy sources used by a thermal prosumer. Various strategies, including heat pump integration, are experimentally studied to improve the prosumer's energy self-consumption in a district heating network operating at two temperature levels (80/50 °C and 60/30 °C for supply and return), utilizing the hardware-in-the-loop technique to couple the substation in real-time with data-driven profiles for thermal loads (multi-family residential buildings) and production (solar panels). Energy flows are analysed for representative days and then extrapolated to calculate yearly results. The implemented strategies were found to be effective in terms of user's self-sufficiency: the energy produced by solar panels and used to cover the thermal demand increased across all case studies i.e., from 8 % to 27 % for non-renovated buildings operating with high-temperature network, from 14 % to 26 % for renovated buildings with low-temperature network. The share of self-consumption increased from 13 % to 30 %, and from 10 % to 15 % respectively, and the production from renewable sources was enhanced (up to 39 %). With net metering, local energy surplus can be utilized beyond production periods, achieving 58 % self-consumption when integrating a heat pump. The results can support stakeholders in developing efficient district heating systems, particularly in the context of potential thermal energy communities.

1. Introduction

The European Union aims to reduce greenhouse gas emissions by 55 % by 2030 and achieve climate neutrality by 2050, as outlined in the European Climate Law [1]. To meet this goal, strict targets require member states to increase the adoption of renewable energy sources (RES), improve energy efficiency, and reduce emissions [2].

Heating and cooling account for nearly half of Europe's total energy demand, exceeding that of fuels, transportation, and electricity [3], and globally, fossil fuels still dominate final energy consumption, with only 24.8 % of heat generated from RES in 2022, making the decarbonization of heating and cooling a pressing challenge [4]. District heating networks (DHN) play a key role in this transition, enabling broader integration of RES and waste heat, whereas decentralized solutions face limitations, particularly in urban areas [5,6]. Europe has around 6,000 district heating and cooling systems supplying 100 million people across 32 countries, with Scandinavia leading the sector, followed by Germany, France, the UK, and the Netherlands [7]. The revised Energy Efficiency Directive (EU/2023/1791) significantly raises EU ambitions in this field,

* Corresponding author.

E-mail addresses: paolo.sdringola@enea.it (P. Sdringola), mauro.pipiciello@eurac.edu (M. Pipiciello), mattia.ricci@enea.it (M. Ricci), federico.gianaroli@enea.it (F. Gianaroli), diego.menegon@eurac.edu (D. Menegon), federico.trentin@eurac.edu (F. Trentin), francesco.turrin@eurac.edu (F. Turrin), biagio.dipietra@enea.it (B. Di Pietra).

https://doi.org/10.1016/j.enbuild.2025.115713

Received 27 December 2024; Received in revised form 18 March 2025; Accepted 4 April 2025

Available online 10 April 2025

Nomenclature

COP	Coefficient of performance
DG	Distributed Generation
DH	District Heating
DHN	District Heating Network
DHW	Domestic Hot Water
HE	Heat Exchanger
HIL	Hardware In the Loop
HP	Heat Pump
HTHP	High Temperature Heat Pump
PV	Photovoltaic
RES	Renewable Energy Sources
s-MFH	small Multi-Family House
SH	Space Heating
TES	Thermal Energy Storage
E	Thermal Energy
M	Flow rate
T	Temperature
S_C	Coefficient of self-consumption of DG
S_S	Coefficient of energy self-sufficiency
$S_{S,el}$	Coefficient of energy self-sufficiency, for cases including HP
U_{ec}	Useful energy coefficient of DG
u_{rel}	Relative measurement uncertainty

aligning with the 2021 Green Deal proposal and emphasizing the role of efficient district heating (DH) in reducing primary energy consumption while integrating RES and waste heat [8]. In Italy, as of December 2023, 434 district heating networks were operational, mainly concentrated in the north and primarily serving residential space heating (SH) and domestic hot water (DHW) needs. However, the integration of RES remains significantly limited, with direct injection at just 2.9 %, while cogeneration continues to dominate at 65.5 % [9]. One of the challenges in integrating RES into DHN is the mismatch between production and consumption and the consequent thermal losses due to heat not consumed locally but injected into the network [10]. Additionally, solar energy—both thermal and electrical—poses a challenge due to its reduced availability during the winter months, when the demand for thermal energy is highest [11]. Consequently, managing the balance between thermal energy supply and demand in DHN is a complex task [12]. To enhance RES integration into DHN, targeted solutions are required, including Thermal Energy Storage (TES) to balance supply and demand, heat pumps (HP) to improve efficiency, and thermal prosumers leveraging bidirectional substations to share surplus energy. Each of these solutions will be explored in detail in the following paragraphs.

Thermal Energy Storage (TES) offers an effective solution to balance heat supply and demand, allowing thermal energy to be stored over different time scales, from hours to days, weeks and seasons [13]. In particular, Seasonal Thermal Energy Storage represents an ideal solution to shift available energy from the period of lower demand to the heating period [14,15]. In the context of district heating applications, there are several types of these systems [16]: aquifer thermal energy storage uses the ability of rock to store heat underground [17]; alternatively, borehole thermal energy storage is often used in areas with limited space or where access to underground aquifers is possible; finally, pit thermal energy storage represents a versatile and low-cost solution, although it may require more space than other types of seasonal storage [18].

TES in DHN can be implemented as a centralized or distributed system: centralized storage reduces heat loss and costs, but limits the flexibility of the network; distributed storage, both at substation and building level, allows smaller pipe sizes and better adaptability during peak loads [19]. Several studies analysed the effect of heat storage integration within DHN demonstrating the potential benefits of this strategy. Romanchenko *et al.* [20] compared centralized storage using hot water tank with building thermal inertia, finding a 1 % cost reduction with inertia and a 2 % reduction with a hot water tank. Manente *et al.* [21] evaluated thermal storage integration in Ferrara's geothermal and waste-to-energy district heating, showing that a 45 MWh storage can improve energy use, save 800,000 m3 of gas annually, and enhance plant efficiency. Turski and Sekret [22] used buildings and the DHN as thermal storage, reducing the source power of central heating by 14.8 %.

Another solution to promote the integration of RES in DHN is the use of heat pumps that can increase the self-consumption of RES and mitigate intermittency, while offering high efficiency for space heating and cooling and hot water production [23,24]. However, the environmental sustainability of heat pumps depends not only on their performance, but also on the type of energy used to generate the electricity needed for their operation [25]. The required electricity can be provided by the grid or generated locally by various RES based technologies such as photovoltaic (PV) cells. In recent years, the advantages of heat pumps in terms of energy efficiency and environmental aspects have been the subject of several studies, especially when they are integrated with PV systems. For example, Alhuyi Nazari *et al.* [26] conducted a review on heat pump systems integrated with PV modules, examining the results obtained from research on this topic. Not only solar electric energy but also solar thermal energy, as a renewable source, can be used to provide the heat needed for the evaporator of HPs. These types of HPs are known as Solar Assisted Heat Pumps and can be configured both in series and in parallel, thus contributing to the heating of buildings [27]. This approach not only mitigates the problems related to the intermittency of solar energy availability, but also increases the overall efficiency in the use of solar energy [28,29].

In this framework, HP technologies represent a promising solution for RES integration within DHN, as they can be installed at different levels: building, network, and plant. Integration at the building level is achieved using small-scale HPs, with effective results depending on the implementation of appropriate business models, as highlighted by Lygnerud *et al.* [30]. Capone *et al.* [31] focused on large-scale heat pumps, which can be installed at the network and plant levels introducing a methodology to evaluate how their benefits differ based on installation location in large DHN. Furthermore, HP represents a promising technology for low-temperature district heating networks, where they can utilize low-temperature heat sources and locally elevate the water temperature for end users. Several studies have explored the integration of heat pumps into these networks, which operate at temperatures below 45 °C. Zhu *et al.* [32] conducted an experimental study to investigate the steady-state thermal behaviour of Booster Heat Pumps under different inlet temperatures and varying flow rates on the user side. Vivian *et al.* [33] examined their performance across supply temperatures ranging from 15 °C to 45 °C, assessing how both supply and return temperatures influence the levelized cost of heat for different end users. Reiners *et al.* [34] used test rigs to investigate HP in ultra-low DHN with a supply temperature of 20 °C, demonstrating that HP can achieve up to twice the efficiency compared to those using geothermal probes. Zhu *et al.* [35] experimentally investigated how refrigerant charge affects temperature, pressure, system coefficient of performance (COP), and heating capacity in these systems proposing a performance-guaranteed range of refrigerant charge to ensure system feasibility. Recent technological developments have extended the operating range of HP, allowing them to reach temperatures up to 140 °C, leading to the classification of high-temperature heat pumps (HTHP) [36]. These HTHPs are a promising and competitive technology for replacing boilers, providing heat up to 180 °C [37]. However, at these high temperatures, ambient air is no longer a feasible heat source for energy-efficient industrial HTHPs. In this context, DHN can be a viable alternative heat source for such applications, with additional potential for integrating HTHPs by using the networks both as heat sinks and sources [38,39].

Another key strategy for RES integration in DHN is enabling connected users to actively contribute to decarbonization by becoming thermal prosumers. Just as in electricity networks, district heating users can not only consume but also produce heat in a decentralized manner, feeding surplus energy into the network. This community-level energy sharing is already well established and regulated at the European level—exemplified by frameworks such as RED II [40,41]. However, although the EU Directives include all forms of renewable energy, a systematic review of the existing literature conducted by Gianaroli *et al.* [42] highlights that the focus is mainly on electric Energy Communities, while the interest in energy communities producing thermal energy is still limited [43]. By converting traditional substations from passive receivers into active bidirectional units, a similar approach can be implemented in DHN to facilitate efficient energy sharing across the community.

Several studies have examined the operation and potential of power-only thermal substations; however, studies on bidirectional substations are still few. Sdringola *et al.* [44] focused on the numerical development of a bidirectional substation for DHN with thermal prosumers, developing and validating in particular a dynamic model using Dymola. This model is based on the experimental results obtained on a prototype substation, as described in the work of Pipiciello *et al.* [45], who conducted dynamic experimental tests, demonstrating that the prototype operated reliably and could handle pressure variations both in the building heating system and in the DHN. Similarly, based on the same prototype, Dino *et al.* [46] developed a dynamic model of the bidirectional substation using TRNSYS, and, in order to demonstrate the potential of the proposed model, a prosumer was applied analyzing the results in two locations with different irradiance values (Palermo and Berlin). The same prototype was the subject of an experimental campaign conducted by Pipiciello *et al.* [47] with the aim of evaluating, on an annual basis, the contribution of a bidirectional substation in optimizing the use of thermal energy produced locally from RES and heat recovery in a high-density population area. The substation was fully integrated in real time with the TRNSYS models of a residential building and a distributed generation (DG) system through the hardware-in-the-loop (HIL) configuration. Testasecca *et al.* [48] developed a thermal network model incorporating various prosumers and dynamically monitored the main thermohydraulic parameters of the network. Rosemann *et al.* [49] presented the results obtained from a control system they developed for a bidirectional substation tested using the HIL technique, while Licklederer *et al.* [50] proposed a control approach combining the assignment of temperature targets to actuators with weighted error functions.

In their 2017 study, Lamaison *et al.* [51] examined the technical specifications and design of solar-powered bidirectional substations, presenting findings from a two-day simulation that highlighted the potential for solar energy reinjection into district heating networks, with measurable contributions to the overall energy demand and efficiency. Later research by the same team focused on testing a bidirectional substation prototype connected to an actual district heating network via a hardware-in-the-loop setup [52]. These 12-day tests revealed suboptimal performance on colder days due to control issues, while the system performed effectively in summer, achieving a solar fraction of 52 %.

In conclusion, among the studies analyzed, the research described by Pipiciello *et al.* [47] represents the most extensive experimental investigation currently documented in scientific literature, having conducted 18 days of testing. This duration and level of detail provide significant insights into the operational performance of bidirectional substations, setting a benchmark for further research in the field. The activities described in this paper build upon the results obtained in that study, which highlighted the potential to increase the local use of heat generated by the solar field, leverage lower temperatures, and minimize unused energy. The findings reveal that the annual contribution of solar-based distributed generation to meeting user demand ranges between 8 % and 14 %, depending on the load levels and the required supply temperatures. In contrast, waste heat offers a significantly higher contribution, reaching up to 41 %, due to a greater temporal alignment between production and demand. However, across all the operational configurations analyzed, an excess production of both solar energy and waste heat was observed, with the surplus being fed back into the network.

Building on these findings, the present paper evaluates technical strategies to increase self-consumption of locally produced thermal energy from RES in a densely populated area, while also considering the possibility for a prosumer to feed surplus energy into the DHN. The analysis considers the challenges posed by the non-simultaneity of energy production and consumption and the potential solutions to mitigate these limitations. The strategies to improve self-consumption were applied to the substation analyzed by Pipiciello *et al.* [47] and experimentally tested at the Energy Exchange laboratory, through six case studies: A1, A2, B1, B2, C, and D. The experimental validation procedure consists of an extensive laboratory campaign with *ad hoc* tests for a DHN operating in two temperature levels, where the bidirectional substation was fully integrated in real-time with TRNSYS models of a residential building (typical small Multi-Family House, before and after renovation) and a distributed generation system using the hardware-in-the-loop technique. The first strategy focuses on managing the discharge temperature of the solar storage and the energy supply temperature from the substation, which was applied in all the case studies. In Cases A1 and B1, this was the only strategy used. The second strategy involves changing the size of the solar storage, applied in Cases A2 and B2. Finally, the third strategy involves integrating a water-to-water heat pump in series with the solar storage, used in Cases C and D.

The methodology and results presented in this paper overcome the limitations of previous studies on prosumers and district heating for several reasons:

- The integration of thermal prosumers and the use of bidirectional substations remains a relatively underexplored area of research. Most existing studies focus on centralized technological solutions, overlooking decentralized ones such as thermal substations, which could play a key role in decarbonizing urban heating sectors.
- The experimental approach in the integration of thermal prosumers is still quite limited. This study stands out for continuing the experimentation of the same system, aiming to achieve the most efficient technological solution through repeated testing and improvements.
- Improving self-consumption through bidirectional substations is tackled from an innovative point of view. While most studies focus on injecting excess energy into the network, the present approach seeks to fully exploit the potential of these substations not only for managing surplus energy, but also for increasing local self-consumption and enhancing the RES production.
- The replicability of the results is another key innovation of this study. The tests were conducted on easily applicable and replicable scenarios across different regions in Italy, thus facilitating the broader adoption of similar solutions in urban and residential contexts.

In summary, this study significantly contributes to the existing literature by proposing innovative solutions for improving self-consumption and integrating renewable energy into urban heating systems, with a specific focus on decentralized, scalable technologies.

The paper is organized into several sections: Section 2 outlines the substation prototype and its control strategies; Section 3 details the methodology, emphasizing the development of system models, setup procedures and the description of the strategies adopted to increase self-consumption; Section 4 offers a comprehensive analysis of test results from each case study on selected days and evaluates the performance of the substation; and Section 5 provides a summary of the conclusions drawn from the modifications made to the system.

2. Prosumer substation description

In this section, the scheme of the prosumer substation and its main features are described. The prosumer substation is designed to operate as a conventional system (using heat exchanger HE1) when locally generated heat is insufficient to satisfy the demand. The heat eventually provided by the local source (through HE2) is primarily self-consumed. If heat production exceeds demand and the temperature requirements are met, the substation is configured to feed the network through HE3. Fig. 1 shows the detailed scheme of the prosumer substation, including the sensors (mass flow, temperature and pressure) and the main components for safety, monitoring and control. The different pipes of the substation, as well as the measurements points are labeled with numbers from 1 to 10. Control strategies are essentially based on managing temperature and flow rates in the various circuits of the substation through the use of motorized valves and the pump: valves C1′, C2′, C4 – these two-way valves primarily control the flow rate in their respective circuits, maintaining it at the predefined set-up values; valves C1, C2 – these three-way valves regulate the flow rate directed to the corresponding heat exchangers (HE1 and HE2), ensuring that the target temperature of the outgoing fluid is achieved; pump P – this variable-speed pump regulates the flow rate drawn from the return branch of the DHN. The control of the valves is determined by the set-up parameters and their corresponding nominal values, as outlined below:

- DG nominal flow rate, $M_{7,nom}$: 3 m^3/h
- Flow rate from the DHN to HE1, $M_{2,nom}$: 1.8 m^3/h
- Nominal flow rate of the user circuit, $M_{8,nom}$: 4.7–3.7–1 m^3/h for a DHN operating at a higher temperature level (80/50 °C for T_1 and T_3); 3.2–2.2–1 m^3/h for lower temperatures (60/30 °C); these three values represent, respectively, the flow rate in case of simultaneous demand for SH and DHW, SH only, and DHW only.
- Return temperature from DHN, $T_{3,nom}$: 50 °C/30 °C
- Minimum temperature difference between DG supply (T_5) and user return (T_8), $\Delta T_{5,min}$: 3 °C
- Substation supply temperature to the DHN, $T_{4,nom}$: 80 °C/60 °C

Further details regarding the sensors, uncertainty measurement, and control strategies are provided in [45] and [47].

3. Test methodology

The test campaign was performed at the Energy Exchange Lab of Eurac Research. This laboratory is equipped with a small-scale DH network, which can emulate both conventional and low-temperature networks by integrating multiple heat sources and users. The test facility is hydraulically connected to the substation and can independently control flow and inlet temperatures in the four interfaces, i.e. points 1, 3, 5, and 8 that are respectively DHN supply, DHN return, DG supply and user return by referring to Fig. 1.

The hardware-in-the-loop technique is adopted so that numerical models dynamically emulate the user's thermal load and the DG heat production profiles. The schematic view of the hardware-in-the-loop implementation is shown in Fig. 2. In the same figure, a red-dashed line indicates the "test boundary", while a green-dashed line indicates the "emulation boundary". The dotted line instead represents the communication between the emulation model and the laboratory facility, while the dotted square and circle indicate the part of the circuit where the strategies are implemented, as described in Section 3.2. The hardware-in-the-loop is implemented so that the supply temperature and mass flow are measured from the substation for each time step and passed as input to the simulation model. Then, the output of the emulation model is passed to the laboratory bench that uses this as

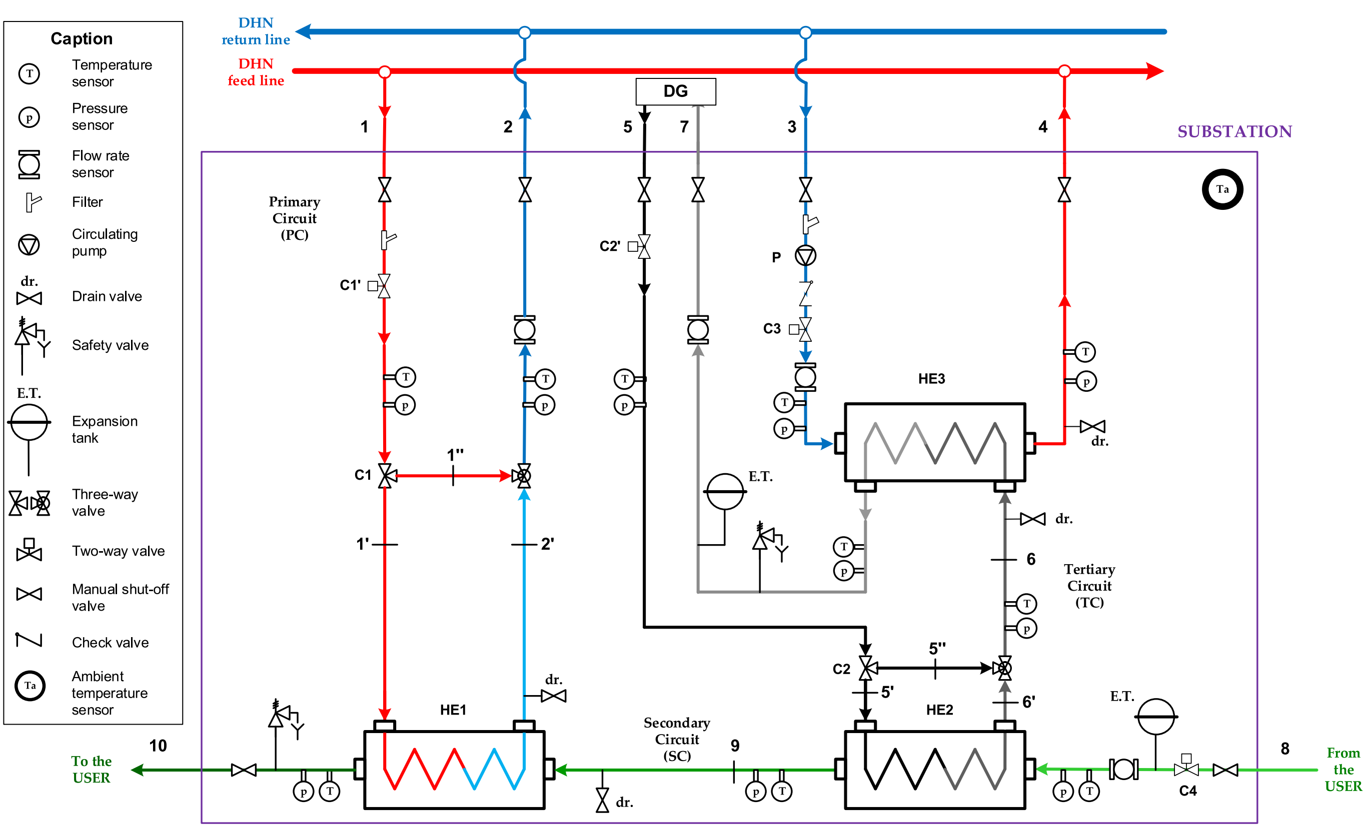

Fig. 1. Schematic layout of the prosumer substation [47].

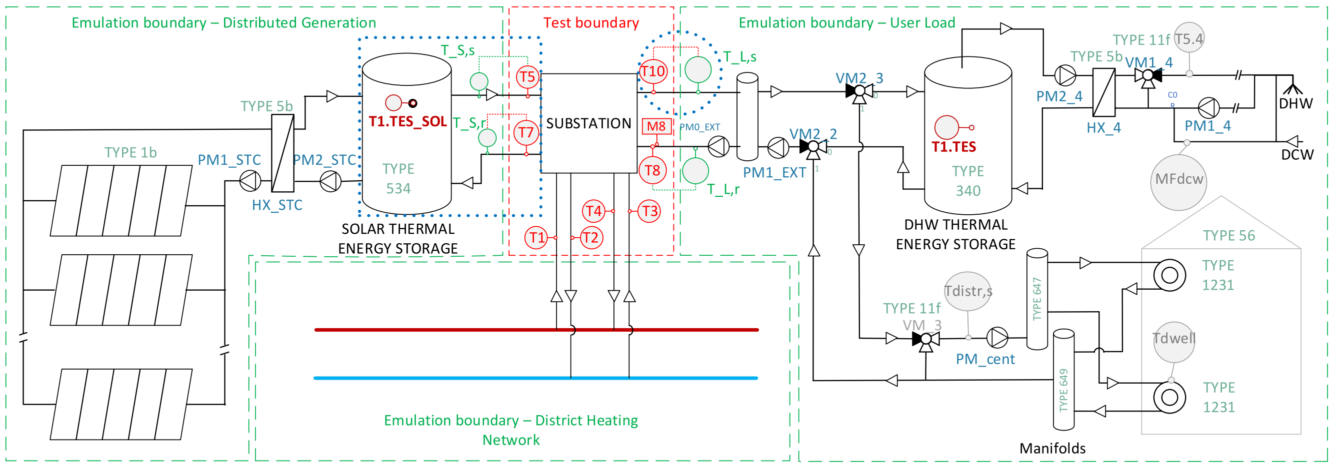

Fig. 2. Hardware-in-the-loop configuration [47].

the reference value for the control of the return temperature.

As regards the emulation parts, TRNSYS is the dynamic simulation software used to emulate the building load and the solar generation.

3.1. Test set-up

LabVIEW® and National Instruments electronics at Eurac Research are used to implement the control and data acquisition systems of the substation. The sampling rate adopted is set equal to one second for all tests. To increase the self-consumption share of RES with respect to what is analysed in [47], 6 case studies are investigated, which main features are shown in Table 1. In this table, for each case, the DHN supply and return temperature are indicated, as well as the temperature T_{10} controls for space heating and domestic hot water, the presence of an emulated HP, the emulated building condition, the number of tested days and the volume of the storage tank dedicated to the emulated solar system. Regarding the DG system, flat plate collectors are considered for all the cases. In order to properly assess the impact of the strategies on the outcomes of the previously mentioned paper [47], the test boundary conditions that are not affected by the strategies remain unchanged. Specifically, the tested days, the DHN temperatures, the solar field and the building models in the current Cases A1, A2, and C are the same as those in the previous paper's Case A (referred to as A0 below). Similarly, the conditions for the current Cases B1, B2, and D are the same as in the previous Case B1 (referred to as B0 below).

To evaluate the substation's performance on a yearly scale, six test days were selected to best represent the variability of climatic conditions throughout the year, following the procedure described in [53]. This procedure involves grouping the days of the year based on daily average temperature and solar irradiation. Each of the resulting six clusters is represented by its medoid. The extrapolation of data to the entire year is performed by weighting the results of each of the six days according to the number of days contained in the corresponding cluster:

$$E_{annual} = \sum_{i=1}^{6} E_i \bullet N_i \tag{1}$$

where E_i is the energy measured on the i-th test day, N_i is the number of days in the i-th cluster, and E_{annual} is the extrapolated annual energy. Table 2 shows the six test days considered, along with their average ambient temperature, average irradiation on horizontal surface, and the number of days belonging to each cluster. Since the greatest benefits associated with the application of the proposed strategies are expected outside the summer season – when solar production is lower and lower thermal levels can be usefully utilized – results from the previous experimental campaign will be referenced for Days 4 and 5 (named A and B in [47], now A0 and B0).

Table 1
Main features of the case studies.

Case study	DHN supply-return temperatures [°C]	T_{10} control for SH	T_{10} control for DHW [°C]	Emulated DG-substation coupling	Emulated building conditions	Number of test days	Solar storage tank [l]
A1	80 – 50	Climatic curve	62	Solar storage tank	not renovated	5	1000
A2	80 – 50	Climatic curve	62	Solar storage tank	not renovated	1	2000
B1	60 – 30	Climatic curve	55	Solar storage tank	renovated	5	1000
B2	60 – 30	Climatic curve	55	Solar storage tank	renovated	1	2000
C	80 – 50	Climatic curve	62	Solar storage tank + HP	not renovated	5	1000
D	60 – 30	Climatic curve	5	Solar storage tank + HP	renovated	5	1000

Table 2
Characteristics of the tested days.

Test day	Day of the year	Daily average ambient temperature [°C]	Daily average irradiation on horizontal surface [W/m^2]	Number of days in the cluster N_i
1	5 January	3.7	63	83
2	21 March	9.9	156	42
3	9 April	15.8	243	47
4	24 May	20.1	153	67
5	1 August	24.4	287	74
6	5 November	10.1	58	52

3.2. Strategies to improve thermal energy production and consumption

In order to increase the self-consumption share from RES of the prosumer, some new strategies are implemented, acting on:

- Temperature control of the solar storage tank discharge and user supply temperature, as described in the Section 3.2.1; this strategy is applied to all the case studies, and it is the only strategy used in A1 and B1.
- Volume of the solar storage tank, as described in 3.2.2; this strategy is implemented in Cases A2 and B2.
- Integration of a HP in the DG system, as described in 3.2.3; this strategy is adopted in Cases C and D.

3.2.1. Temperature controls

In the previous research activity [47] the discharge of the emulated solar storage was dependent on the DHN supply temperature (60 °C and 80 °C for the two cases considered) and activated only for tank temperatures higher than the mentioned value. In the present work, instead, the discharge temperature has been reduced based on the return temperature from the user, so that the heat exchange in HE2 is activated if $T_5 > T_8 + 8^{\circ}C$ and it is deactivated when $T_5 < T_8 + 3^{\circ}C$. This strategy involves the circuit in the dotted blue square in Fig. 2.

Furthermore, in the experimental tests described in [47], the user supply temperature T_{10} was controlled to a constant value set to satisfy the load in all the expected operating conditions. In the present work, instead, the T_{10} set point value is variable, and it depends on both the SH climatic curve and the DHW request according to what is reported in Table 3. This modification involves the circuit in the dotted blue circle in Fig. 2. As regards the control of the heat exchange in HE3, the same control described in [47] is adopted.

3.2.2. Solar storage tank volume

Another technique adopted to increase the self-consumption share from RES of the prosumer is the change in the solar tank volume in the dotted blue square in Fig. 2. Indeed, an increase in the solar storage tank volume is expected to increase the self-consumption share from RES, particularly during winter days. Therefore, in this research work for case studies A2 and B2, the solar tank volume is increased from 1000 l to 2000 l. The selection of the test day to be repeated with increased TES volume is based on an analysis of the experimental results from Cases A1 and B1. The main objective of increasing the TES volume is to enhance the self-consumption share from RES by reducing the amount of energy supplied to the DHN. This goal can be effectively achieved on winter days with energy fed into the DHN between 12 a.m. and 2p.m. (time frame with high solar production and lack of user thermal demand for SH) and minimal solar energy self-consumption from 2p.m. to 10p.m. Only Day 1 of Case B1 meets these criteria among all the days tested. For other days, either no energy is fed into the DHN (mainly in Case A1) or solar energy sufficiently meets the space heating load from 2p.m. to 10p.m. (notably for Days 2, 3, and 6 in Case B1). On Day 1 of Case B1, the energy supplied to the DHN is 24 kWh. To store this energy at a temperature level that prevents it from being fed into the DHN, a storage volume of 4000 L has been estimated as necessary, corresponding to 400 % of the current TES volume. On one hand, such a substantial increase in volume is considered incompatible with the dimensions of the substation and any potential refurbishment of the existing setup. On the other hand, an increase of less than 100 % has been assessed to have limited effects on self-consumption. Therefore, the authors decided to initially increase the TES volume by 100 %, leaving the possibility for further increases if no significant improvements are observed.

Table 3
T_{10} set-point values based on SH climatic curve and DHW request.

Case study	SH climatic curve	DHW storage tank charge temperature
A	60 °C @ −7 °C, 40 °C @ 20 °C	62 °C
B	55 °C @ −7 °C, 30 °C @ 20 °C	55 °C
C	60 °C @ −7 °C, 40 °C @ 20 °C	62 °C
D	55 °C @ −7 °C, 30 °C @ 20 °C	55 °C

3.2.3. Integration of a heat pump in the DG system

A water-to-water heat pump has been emulated and connected to the solar storage tank. This configuration has been tested in case studies C and D. The integration of the HP involves the circuit in the dotted blue square in Fig. 2. Fig. 3 shows a zoom of the mentioned part with a detailed scheme on the integration of the HP. The interaction between emulation and test boundaries follows the same approach described in Section 3. The HP has been designed to i) increase the self-consumption of solar energy for space heating load, ii) have a stable and continuous operation; the HP typology, in terms of size and operating conditions, is not aimed at feeding the DHN. These assumptions are the basics to define the HP features described in the Section 3.3, and to detail the following controls.

Two different working logics are implemented to manage the integration of the HP based on the temperature of the solar storage tank and the return temperature from the user (T_8):

- HP bypass and so direct heat transfer between the DG and the substation;
- HP activation so that the evaporator is connected to the DG and the condenser to the substation.

The motorized valves VM4_1, VM4_2, VM4_3, VM4_4 in Fig. 3 allows to properly set the hydraulic configuration for two operating modes.

In order to implement these working logics, several control variables are considered:

- return temperature from the user, T_8;
- user flow rate, M_8;
- solar storage tank temperature at its top, $T1.TES\_SOL$;
- minimum inlet temperature of the evaporator (10 °C), $T1.TES\_SOL\_min$;
- minimum temperature difference between HE2 inlets ($T_5 - T_8$) to have a valuable and stable heat exchange, $\Delta T_{5,min} = 3^{\circ}C$;
- maximum solar storage tank temperature to activate the HP, $T1.TES\_SOL\_max$, that equals $T_8 + \Delta T_{5,min}$;
- outlet set-point temperature at the condenser, $T\_HP\_SP = 55^{\circ}C$;
- cost of electricity, c_el, 0.2524 €/kWh (typical household consumer under protection service, contracted power 3 kW and annual consumption 2700 kWh, Q1 2024, defined by Italian Regulatory Authority for Energy, Networks and Environment ARERA);
- cost of thermal energy from DHN, c_th, 0.1765 €/kWh (single-rate domestic tariff, contracted power ≤ 30 kW and annual consumption ≤ 25,000 kWh, Q1 2024, determined by the company providing the district heating service in the area under consideration, as there are currently no national reference standards).

The implemented control logic activates the HP when the following conditions are satisfied at the same time:

- $T1.TES\_SOL < T_8 + \Delta T_{5,min} < T\_SP\_HP$, so it would not be possible to supply energy to the load bypassing the HP that could give its contribution;
- $M_8 > 0$, so there is a user heat demand;
- $T1.TES\_SOL > T1.TES\_SOL\_min$, so it is technically possible to start the HP;
- the COP of the HP is higher than c_el/c_th, so it is economically more convenient to use the HP instead of the heat for the DHN.

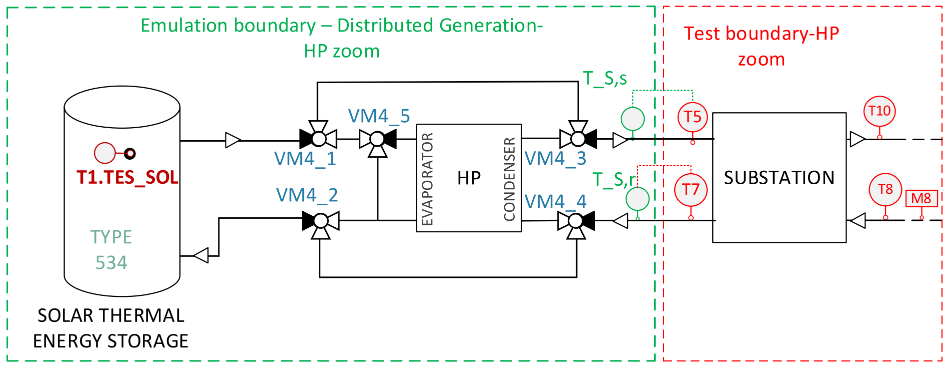

Fig. 3. Integration of a heat pump in the DG system.

Regarding the bypass of the HP, it is activated when the following conditions are satisfied at the same time:

- $T1.TES\_SOL > T_8 + \Delta T_{5,min}$, so it is possible to use energy from the solar storage directly;
- $M_8 > 0$, so there is a user heat demand.

3.3. Numerical model

Numerical simulations are performed using the software TRNSYS. The numerical model used for the hardware-in-the-loop implementation represents a small Multi-Family House (s-MFH) with two dwellings per floor (floor area of 50 m^2) and five floors. The building model considered in Cases A0-A1-C represents a typical s-MFH built in the European Continental climate, as defined in [54]. The yearly thermal energy consumption results are considered representative of realistic scenarios, having been validated against statistical data [54]. The DHW demand has been generated with the software DHWCalc [55]. The building model used in Cases B0-B1-D is identical to that of Cases A0-A1-C in terms of geometrical features, the user demand side hydraulic circuit, and emission terminals (radiators). The building's thermal envelope was improved by adding a layer of thermal insulation (polystyrene) to the external walls and to the flat roof, with an 8 cm thick insulation layer applied in both cases. In addition, the windows were replaced with others presenting lower thermal transmittance values. These modifications are typical for energy refurbishments of this type of building. They help reduce the building's thermal load, allowing to lower the supply water temperature distributed to the radiators and ensuring the same users' thermal comfort.

For further details on the building modelling the reader is invited to refer to [47]. Regarding the climatic conditions, Bologna has been used as reference location in this work.

Regarding the numerical modelling of the flat solar thermal collectors a total surface of 110 m^2 is considered with a thermal efficiency at nominal conditions equal to 0.61, having a solar system thermal power at nominal conditions similar to the thermal power delivered by the substation at nominal conditions (60 kW). For further details the read is referred to [47].

Regarding the HP, an *ad hoc* numerical model is developed by Eurac Research by means of a dedicated TRNSYS type aiming to meet the design objectives mentioned in the Section 3.2.3. The main characteristics of the HP implemented are shown in Table 4.

Table 4
Main characteristics of the emulated HP used in case studies C and D.

Quantity	Values
Thermal power range (condenser) in design conditions [kW]	2–8
COP range in design conditions	6.0–4.5
Minimum evaporator inlet temperature [°C]	10
Maximum evaporator inlet temperature [°C]	40
Maximum condenser outlet temperature [°C]	55

The HP is designed to modulate the thermal power in the 2–8 kW range when the temperature at the evaporator inlet is 25 °C and the condenser outlet temperature is 45 °C. The lower value corresponds to the minimum load required by the building on tested spring day (Day 3). Hence, it has been chosen to guarantee a continuous operation of the HP and avoid intermittency. Modulation is possible in the range of 25 % to 100 %, resulting in a corresponding maximum thermal power of 8 kW. Regarding the design temperatures, the evaporator inlet temperature is set as the average of the minimum (10 °C) and maximum (40 °C) allowed temperatures for the selected HP. Similarly, the condenser temperature is set as the average of the maximum allowed temperature (55 °C) and the expected minimum temperature (35 °C) to ensure effective heat exchange in HE2, based on the analysis of the previous test campaign.

The numerical model of the HP is implemented so that:

- it is equipped with a variable speed compressor in order to control the condenser outlet temperature at the set point value;
- the mass flow rate in the heat source circuit is varied to maintain a minimum temperature difference of 5 °C between inlet and outlet;
- the maximum inlet temperature at the source side is limited to 40 °C (maximum allowable inlet temperature) through the valve VM4_5 in Fig. 3.

3.4. Calculations and KPI

In order to compare results obtained for each case study, the following KPIs are adopted:

- S_C, that represents the coefficient of self-consumption of DG;
- S_S, that represents the coefficient of self-sufficiency;
- U_{ec}, that represents the useful energy coefficient of DG.

The aforementioned KPIs are defined as follows:

$$S_C = 100 \bullet \frac{E_{DG\ to\ user}}{E_{DG}} \tag{2}$$

$$S_S = 100 \bullet \frac{E_{DG\ to\ user}}{E_{User}} \tag{3}$$

$$U_{ec} = 100 \bullet \frac{E_{DG\ to\ user} + E_{DG\ to\ DHN}}{E_{DG}} \tag{4}$$

where:

- E_{DG} is the thermal energy produced by the DG system;
- $E_{DG\ to\ DHN}$ is the thermal energy produced by the DG system and injected into the DHN;

- E_{User} is the thermal energy demand of the user;
- $E_{DG\ to\ user}$ is the thermal energy produced by the DG system and sent to the user.

In the cases without the HP (A and B) $E_{DG\ to\ user}$ represents the thermal energy exchanged in HE2. When the HP is present (C and D) instead $E_{DG\ to\ user}$ is defined as follows:

$$E_{DG\ to\ user} = \left(E_{DG\ bypassHP} + E_{condHP}\right) - E_{elHP} \quad (5)$$

where $E_{DG\ bypassHP}$ is the thermal energy provided to the user by the DG system and hence bypassing the HP, E_{condHP} is the thermal energy provided to the user by the HP, and E_{elHP} is the electric energy absorbed by the HP.

In cases with HP (C and D), it is also calculated the coefficient $S_{S,el}$, which is valid in case the HP is fed by electricity produced locally by RES:

$$S_{S,\,el} = 100 \bullet \frac{E_{DG\ to\ user} + E_{elHP}}{E_{User}} \quad (6)$$

4. Test results and discussion

In this section, the substation performances for different case studies (from A to D) and each representative day (from 1 to 6) are presented and discussed. The main variables of the substation have been monitored and sampled with a 1-sec time step; moreover, the hardware-in-the-loop configuration introduced user demand and DG production profiles allowing to characterize the device under operational conditions. The prototype response in terms of energy exchange within its HEs was verified according to the following commands: i) thermal request by the user to meet heating needs (the heating schedule is from 6 a.m. to 12 a.m. and from 2p.m. to 10p.m.); ii) thermal demand by the user to charge the DHW storage tank (which is activated when the temperature inside, at the height of about 60 % from the bottom, reaches 55 °C and 48 °C and remains active until the temperature reaches 60 °C and 53 °C, for Cases A-C and B-D, respectively); iii) the availability of solar energy at a temperature useful for meeting the user's thermal demands or for feeding the DHN, resulting in the discharge of the storage tank connected to the solar circuit. Section 4.1 provides a detailed description of the results obtained from tests on two of the six representative days: Day 1, typically winter, and Day 3, representing the mid-season, specifically spring; these are the two extreme cases of the space heating season showing a different effect of the proposed strategies. Section 4.2 describes the daily energy balance and the application of a net metering option, while the relative annual extrapolations are included and commented in Section 4.3.

4.1. Results for Day 1 and Day 3

The results for two representative days are described below: Day 1, 5 January, and Day 3, 9 April. Fig. 4 shows the Global Horizontal Irradiance and the outdoor temperature for the two selected days. The interaction between the three HEs to meet the user's thermal load and feed energy into the grid is depicted for Day 1 in Fig. 5 and Fig. 6. Fig. 5 refers to a traditional DHN (80/50 °C for supply and return) and a not renovated building. It gathers results from the previous experimental campaign (named A0) and the current case studies A1 and C. Fig. 6 instead refers to the experimental tests related to lower-temperature DHN (60/30 °C for supply and return) and a renovated building, showing results from the previous campaign (named B0) and the current case studies B1 and D. In order to improve the readability of the paper, Authors chose to place the figures corresponding to Day 3 in the appendix (Fig. 11 and Fig. 12). Comparing within the same graph the results obtained in different tests with the same boundary conditions allows to highlight the effects of the implemented strategies aimed at increasing self-consumption. Finally, for a better understanding of the results discussed below, in terms of user thermal load coverage and distribution of DG energy, refer to Fig. 7 and Fig. 8.

The above-mentioned figures illustrate how the three heat exchangers, HE1, HE2, and HE3, work together to meet the load and supply energy to the grid, depending on the user's thermal demands and the availability of solar energy. The lower graphs display two of the three mentioned commands determining the activation of the substation (binary signals): the DHW storage charge and the availability of useful solar energy in the solar storage. For Cases C and D, the useful solar energy availability curve comprises of two contributions: the solar storage used as a source for the heat pump, which in turn supplies HE2; direct use of the energy in the solar storage (bypass) for both HE2 and HE3. The upper graph depicts the heat power supplied by the substation to the user via HE1 (DHN) and HE2 (DG) i.e., overall user demand for SH and DHW. The separate contributions of the two heat exchangers and the heat supplied by HE3 to the district heating network are shown in the middle graphs. The user demand and the available DG (solar) energy fluctuate in each test according to the emulation output. Finally, note that when starting up the substation, or charging the DHW storage, or starting solar availability, exchanged thermal powers suddenly increase due to both dynamic changes in temperature and flow rate typical of start-up, and an actual increased demand from the user related to DHW storage charging. The user's thermal energy demand varies between 5 and 40 kW: in Cases A0 and A1, where a non-refurbished building is emulated, the SH load profile varies between 5 and 30 kW, in Cases B0 and B1 between 5 and 15 kW; the DHW causes peaks in the overall load.

In the cases of non-refurbished building (A0-A1-C), test day 1 is characterized by high user demand for SH (244 kWh), being included in

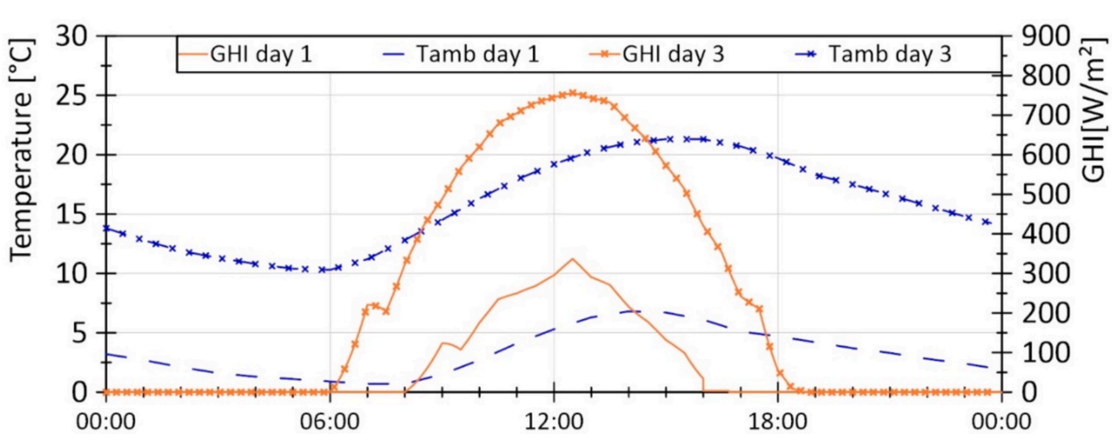

Fig. 4. Global Horizontal Irradiance (orange line) and outdoor temperature (blue dashed line) for Day 1 and Day 3. (For interpretation of the references to colour in this figure legend, the reader is referred to the web version of this article.)

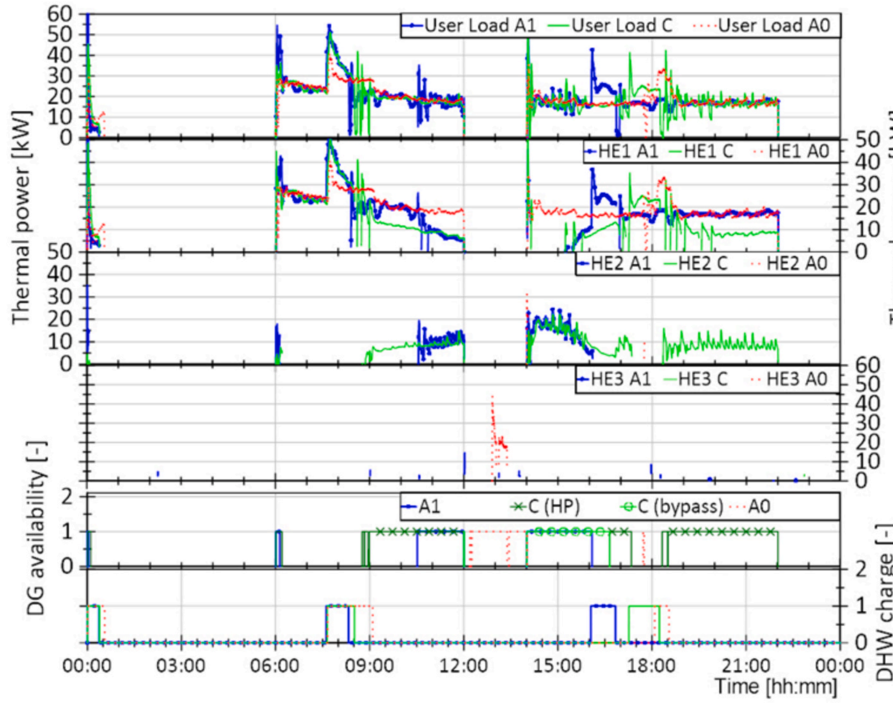

Fig. 5. Day 1. Interaction between the HEs according to thermal demand and DG availability. Case studies A0-A1-C, DHN supply and return 80/50 °C.

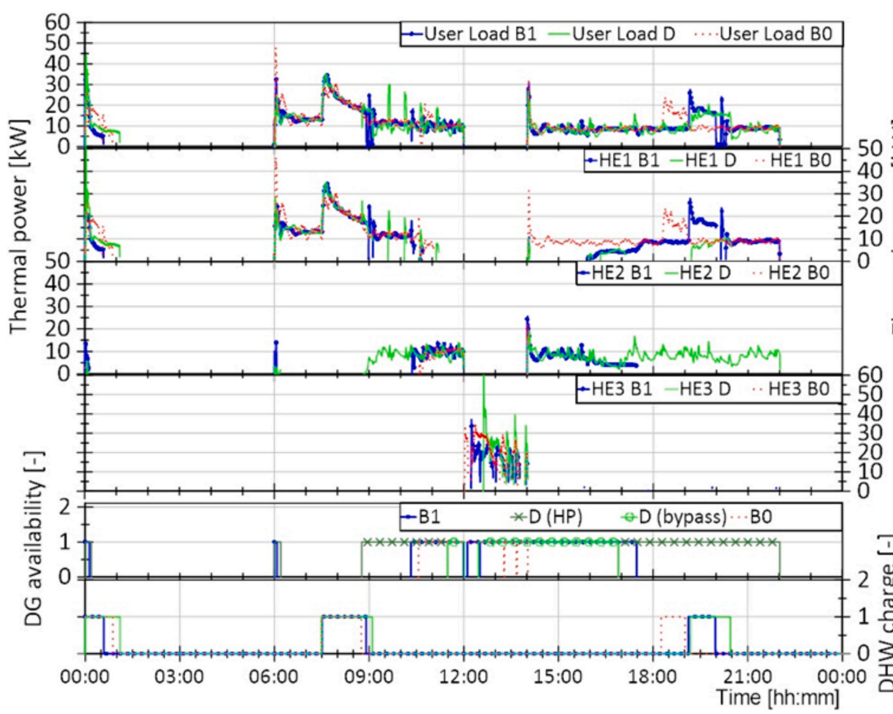

Fig. 6. Day 1. Interaction between the HEs according to thermal demand and DG availability. Case studies B0-B1-D, DHN supply and return 60/30 °C.

the heating period, and DHW (20 kWh) alongside low solar radiation. Fig. 5 shows that the user's thermal demands are almost exclusively supplied from HE1, so from the DHN, in both experimental campaigns A0 (99.8 %) and A1 (87.1 %). In Case A0, the availability of solar energy is simultaneous with the thermal demand only to a small extent: thus, during the central hours of the day just a little part of user's demand is supplied from the solar panels (0.2 %, equivalent to the 2.3 % of the energy produced by solar), with HE2 activated twice for approximately 3 min. The remaining useful solar energy availability is fed into the DHN via HE3 (30.8 % of the energy produced by solar), when there is no demand around 12:50 and 13:30. Strategies for increasing self-consumption described above for Case A1 made solar energy available in the solar storage with a good phasing with user's demand: it is satisfied by HE2 completely or partially (12.9 % of the daily user's demand, equivalent to the 68.4 % of the energy produced by solar), thus leading the simultaneous activation of HE1 and HE2. Differently from Case A0, HE3 does not operate because the temperature in the solar storage remains below the minimum threshold temperature for its activation (83 °C). With the integration of a heat pump (Case C), the user's demand is addressed by HE1 (75 %) and HE2 (25 %, equivalent to 64.4 % of the energy produced by solar) for comparable durations, including periods of simultaneous operation. HE1 meets the thermal load during the early hours, when the solar storage lacks usable energy, and during the final DHW charge. HE2 operates from 9:00 to 22:00, phasing with the user's SH demand: 64.6 % of energy exchanged in HE2 is from the heat pump that operates in the morning, when solar energy production is increasing and the temperature in the solar storage is insufficient to activate the bypass, and from 17:00 onwards, when solar energy production ceases, but the storage temperature remains sufficient for heat pump activation; from 14:00 to 16:00, HE2 is directly fed from the solar storage (bypass activated, 35.4 % of energy exchanged in HE2) and can independently meet the load. Additionally, during the final DHW charge, HE2 stopped working to accommodate the charging process because the temperature T_8 was higher than the HP set point temperature: with the set point equal to the maximum condenser outlet temperature, the HP could not contribute to the load in this operating condition. As for Case A1, HE3 also does not operate in Case C because the temperature in the solar storage is under the threshold to feed energy into the network.

By testing Day 1 of Case A1 with a doubled solar storage volume (i.e., Case A2, not shown in the following figures for reasons of clarity in the graphic representation), the substation operates similarly to Case A1. The user's demand is primarily supplied by the DHN via HE1 (87.1 % in A1, 84.8 % in A2), then by solar energy via HE2 (12.9 % in A1, 15.2 % in A2), with no feed-in to the grid. The share of the energy produced by solar stands at 68 %; the difference in the useful solar energy feeding HE2 is attributed to the increased solar production, which rises from 53.4 kWh (A1) to 62 kWh (A2), resulting from the higher efficiency of the solar array. In Case A2, the presence of a double storage system results in a lower temperature in the solar storage, a lower average operating temperature of the solar array, and thus a higher production efficiency.

Moving to lower operating temperatures in DHN and a renovated building as user (Cases B0-B1-D), SH demand decreases to around 130 kWh, while the DHW demand remains constant. Fig. 6 shows that even in this scenario the user's thermal demands are primarily supplied from HE1 (B0 92.8 %, B1 84.1 %). In Case B0, the availability of solar energy is partly at the same time as the user's demand, thus between 11:30 and 12:00 a portion of the thermal power required by the user is supplied by the solar plant via HE2 (7.2 %, equivalent to 22.6 % of the energy produced by solar); the remaining useful solar energy availability is fed into the DHN through HE3 (56.5 %), which operates from 12:00 to 14:00. Implementing the strategies for increasing self-consumption described above for Case B1, more solar energy is available in the solar storage at the same time as the user's demand. This results in the operation of HE1 alone, or in combination with HE2 (overall 15.9 % of the demand, equivalent to the 40.4 % of the energy produced by solar); additionally, HE3 operates on its own when there is no demand from the user (36.4 % of solar production fed into the network). With the integration of a heat pump, Case D shows an operation similar to Case B1: user's demand addressed by HE1 (65.4 %) and HE2 (34.6 %, equivalent to 52 % of the energy produced by solar) with either solo or simultaneous operation; HE1 meets the load during the early hours of the day and during the final DHW charge, coupled with HE2; HE2 operates from 9:00 to 22:00, phasing with the load profile and covering the user's demand mainly on its own, whether powered by the heat pump (68 % of energy exchanged in HE2) or directly from the solar storage (bypass activated, 32 %). HE3 operates during the middle part of the day (24.5 % of the solar production fed into the network), when there is no demand from the user and not simultaneously with HE2.

By testing Day 1 of Case B1 with a doubled solar storage volume (i.e., Case B2), the substation still operates similarly to Case B1. HE1 covers a significant amount of user's demand using the DHN (84.1 % in B1, 77 % in B2), while the useful solar energy is partially consumed via HE2 and fed into the network via HE3 (40.4 % in B1 and 52 % in B2, and 36.4 % in B1 and 18.3 % in B2, respectively; these shares refer to the energy produced by solar). The difference in the useful solar energy feeding HE2 is related to the higher solar production (66.3 kWh in B1 and 73.9 kWh in B2) and to a lower amount of energy fed into the grid (24.1 kWh in B1 and 13.5 kWh in B2), caused by a lower temperature in the solar storage.

Test day 3 is in mid-season (April), still in the heating period. In the case of non-refurbished building (Cases A0-A1-C), the thermal demand for DHW is 30 kWh and for SH is 100 kWh, 60 % lower than test day 1. The solar production reaches 233 kWh (more than four times higher if compared to test day 1), thus letting expect a significant exploitation of solar energy. Fig. 11 shows that the user's thermal demands are primarily supplied from HE1, so from the DHN, in both experimental campaigns A0 (72 %) and A1 (54.6 %). In Case A0, HE2 operates at the same time as HE1 between about 09:00 and 09:40, with comparable powers; thereafter (09:40–12:00 and 14:00–17:00) it runs alone, and then switches off due to exhaustion of solar availability. Overall, DG via HE2 supplies 28 % of the user's demand, equivalent to 20 % of the energy produced by solar; the remaining useful solar energy is fed into the DHN via HE3 (69 %), which works both coupled with HE2 (10:00–12:00 and 14:00–16:00) and on its own (12:00–14:00). After implementing the strategies for an improved self-consumption for Case A1, the user's thermal demands are supplied from HE2 (45.4 %, equivalent to the 29.1 % of the energy produced by solar) for much of the time; HE1 operates in the first part of the day, when there is no solar availability, and during the last DHW charge. The remaining useful solar energy availability is fed into the DHN via HE3 (56.4 %). With the integration of a heat pump (Case C), the user's demand is addressed by HE1 (54.4 %) and for much of the time by HE2 (45.6 %, equivalent to 25.6 % of the energy produced by solar, now reaching 258 kWh). HE1 works during the DHW charges and coupled with HE2 for some periods at the beginning of the SH. Out of this simultaneous operation, HE2 meets the SH demand on its own, even when operating with the heat pump (06:00–08:00, 15.3 % of energy exchanged in HE2), unlike test Day 1, as the demand is lower. During the remaining heating period, HE2 is fed directly from the solar storage (bypass activated, 84.7 % of energy exchanged in HE2). In addition, HE3 also operates partly simultaneously with HE2 and partly alone, when there is no demand from the user, resulting in 54.3 % of the solar production fed into the network.

Focusing on lower operating temperatures in DHN and a renovated building as user (Cases B0-B1-D), SH demand decreases to around 23 kWh, while the DHW demand remains constant. As shown in Fig. 12, even under the above-mentioned boundary conditions, the user's thermal demands are mainly supplied from HE1, so from the DHN, in both B0 (69 %) and B1 (73.5 %). In Case B0, part of the thermal power required by the user is supplied by the solar system via HE2 (31 %, equivalent to 8.6 % of the energy produced by solar), between approx. 09:00 and 17:00. During the same time interval, the remaining useful solar energy availability is fed into the DHN via HE3 (84.2 %), either in combination with HE2 (09:00–12:00 and 14:00–17:00) or alone (12:00–14:00) when there is no user demand. The strategies for increasing self-consumption in Case B1 resulted in a user's demand satisfied most of the time by HE2 (26.5 %, equivalent to 6.4 % of the energy produced by solar); HE1 operates in the first part of the day, when there is no solar availability, and during the last DHW load. HE3 is activated either coupled with HE2 and alone (80.2 % of the solar production fed into the network), when there is no user demand. A comparative analysis of the results obtained for Cases B1 and B0 reveals no increase in the self-consumption of the DG energy. This can be attributed to the operational conditions on Day 3 (lower-temperature DHN and an energy demand from a renovated building covered by lower thermal levels), which reduce the potential of the expected benefits related to the proposed strategies, if compared to winter scenarios. Furthermore, it is important to consider the challenges in ensuring full repeatability of the dynamic tests performed in the laboratory; it is intrinsically linked to the nature of the devices tested and their operational behavior, which is influenced by variations in operating conditions that cannot be entirely controlled. For these reasons, the benefits associated with the implementation of the strategies do not manifest, while observing an increase in solar production and a higher amount of useful solar energy. With the integration of a heat pump (Case D), the user's thermal demands are supplied from HE1 (65.8 %) and from HE2 (34.2 %, equivalent to the 6.3 % of the energy produced by solar) for much of the time; HE1 is activated in the first part of the day, when there is no solar availability, and together with HE2 during the last DHW charge. HE2 operates from 07:00 to 22:00, phasing with the load profile and covering the user's demand mainly on its own, whether powered by the heat pump (21.1 % of energy exchanged in HE2, 07:00–09:00) or directly from the solar storage (bypass activated, 78.9 %). HE3 operates during the middle part of the day (76 % of the solar production fed into the network), when there is no demand from the user or simultaneously with HE2.

The experimental test campaigns conducted for Cases A, B, C, and D, along with those indicated in [47], confirm the efficacy of the controls implemented on the substation. These controls successfully maintained the required supply temperature for the user (T_{10}) and the input temperature of the DHN (T_4), with only minor deviations observed around the set-point.

4.2. Daily results and net metering option

This section presents a comparison of the different case studies with the same load type across the six representative days: A0-A1-C in Fig. 7, and B0-B1-D in Fig. 8. As introduced in Section 3.1, test Days 4 e 5 were not performed for case studies A1, B1, C, and D; results from the previous experimental campaign were used as reference for the full-year extrapolation (Section 4.3). The top graph in both figures illustrates the daily user load and the contributions from DHN (HE1) and DG (HE2), including the KPIs related to energy self-sufficiency (S_S and $S_{S,el}$), as defined in Section 3.4. The total energy load observed for each individual day across the three cases is similar but not identical, due to the abovementioned dynamic and non-repeatable nature of laboratory testing. The bottom graph in both figures shows the total energy from DG, along with its distribution to the user via HE2, to the DHN via HE3, and the energy not used; additionally, the figure includes the S_C and U_{ec} indicators, as defined in Section 3.4. The total energy from DG also includes the electrical consumption of the HP during Case C, considered an energy input to the control volume used for evaluating DG production and usage (whose boundaries encompass the solar circuit heat exchanger in the numerical model, HE2, and HE3). The share of energy produced by the DG and not used for supplying the user or feeding the network is related to the following contributions: preheating of the solar circuit, crucial for bringing the system into storage loading conditions (the energy required remains relatively constant, e.g. ranging from approximately 5 to 7 kWh for Case A1 and 2.7 to 4.4 kWh for Case B1); variable share based on the operational conditions of the solar system, which include the preheating of the solar storage, thermal losses (from storage, the circuit between storage and the substation, and HE), as well as the energy remaining in storage and not utilized by the user.

As for the experimental campaigns of case studies A1 and C (Fig. 7), Days 1 and 6 represent typical winter days, characterized by high user load for SH and DHW, and low solar radiation: user demand is predominantly supplied by the DHN (87.1 % and 86.4 % in A1; 75 % and 73.5 % in C, respectively); energy from DG is self-consumed by the user through HE2, with no surplus fed into the grid; in Case C, HE2 is supplied both from solar storage (35 %) and the HP (65 %). The DG energy not used is approximately 32 % for Day 1 and 28 % for Day 6 in A1 (16.9 kWh and 12 kWh, out of a total production of 53.4 kWh and 42.6 kWh respectively), mainly due to thermal losses and preheating in the various circuits. This percentage increases to 36 % for Day 1 and 44 % for Day 6 in Case C (32.3 kWh and 35.9 kWh, out of a total production of 90.9 kWh

Test day	1	1	1	2	2	2	3	3	3	4	5	6	6	6
	A0	A1	C	A0	A1	C	A0	A1	C	A0	A0	A0	A1	C
from DG	1	37	70	17	55	78	45	68	70	5	11	10	31	56
from DHN	286	247	209	186	156	131	115	82	83	25	16	219	194	156
Tot	287	284	279	203	210	209	160	149	153	30	27	229	224	213
Ss	0%	13%	21%	8%	26%	34%	28%	45%	43%	16%	40%	4%	14%	22%
Ss,el			25%			37%			46%					26%

Test day	1	1	1	2	2	2	3	3	3	4	5	6	6	6
	A0	A1	C	A0	A1	C	A0	A1	C	A0	A0	A0	A1	C
Not used	18	17	32	15	19	42	25	34	52	11	24	14	12	36
to DHN	8	0	0	18	3	0	155	131	140	14	191	0	0	0
to user	1	37	70	17	55	78	45	68	70	5	11	10	31	56
Tot	27	53	102	50	76	120	225	233	261	30	225	24	43	92
Sc	2%	68%	64%	34%	72%	63%	20%	29%	26%	16%	5%	42%	72%	56%
Uec	33%	68%	64%	70%	75%	63%	89%	86%	80%	63%	89%	42%	72%	56%

Fig. 7. User load sharing between DHN and DG, distribution of DG energy production, and KPIs for the representative days. Case studies A0-A1-C.

and 81.6 kWh respectively), because of additional energy produced during the day which remains unused in the storage at the end of the day (at a temperature level that can still be utilized by the HP).

Days 2 and 3 are spring days characterized by good solar radiation and simultaneous thermal demands for SH and DHW: user's thermal demands are met by the DHN (73.9 % and 54.6 % in A1; 62.7 % and 54.4 % in C, respectively); on Day 3, solar production is approximately 2 to 3 times higher than on Day 2 for Cases C and A1, respectively, leading to a correspondingly higher fraction of solar energy supplied to the building; on Day 3, solar energy is actually fed into the DHN, accounting for more than 50 % of the total solar energy production. In Case C, HE2 is supplied both directly from solar storage via the bypass (38.3 % and 84.7 % for Days 2 and 3, respectively) and by the HP (31.7 % and 15.3 %); the heat pump plays a lesser role on Day 3 due to the higher availability of solar energy from increased solar radiation. In Case A1, on Day 2, 25 % of DG energy remains unused (18.9 kWh out of a total production of 76.4 kWh), mainly due to thermal losses and preheating in the various circuits; on Day 3 (14 %, 33.9 kWh out of a total production of 233 kWh) it includes part of the energy remaining in storage at the end of the day. A similar behavior is observed in Case C, with unused DG energy accounting for 37 % on Day 2 (42.4 kWh out of a total production of 113 kWh), and 20 % on Day 3 (51.8 kWh out of a total production of 257.6 kWh); in both cases, the energy remains not used in storage at the end of the day but at a temperature level that can still be utilized by the heat pump.

The insights regarding the substation qualitative behavior on the representative days described above can be considered almost entirely valid for the cases of lower operating temperatures in DHN (B1-D, Fig. 8). A difference is observed for Days 1 and 6, when the energy produced by solar DG is both self-consumed by the user via HE2 and fed into the grid via HE3.

Comparing all the case studies A0-A1-C (Fig. 7), user demand is mainly met by the DHN (from 54.6 % for Day 3 A1, up to 99.8 % for Day 1 A0); only Day 3, Cases A1 and C, shows comparable shares from DG and DHN. The figure further indicates that the contribution to the user from DG increases during the tested days as the case studies progress from A0 to C, particularly on days with higher user demand (i.e., Days 1, 2, and 6). The increase in solar output from A0 to C is due to the gradual reduction in the operating temperature of the solar storage, which results from the lower temperature required to supply the DG side of the substation. Consequently, the average operating temperature of the solar array also decreases, leading to improved performance.

Moving to case studies B0-B1-D, Fig. 8 confirms that DHN mainly contributes to covering the user demand (from 55.1 % for Day 5 B0, up to 100 % for Day 4 B0). For the same reasons described above, the solar output increases from B0 to D. The contribution to the user from DG by HE2 increases again during the tested days; it is more pronounced and evident on days with higher user demand (i.e., Days 1, 2, and 6), and less on Day 3, characterized by low user demand during the central and late hours of the day, when solar energy is available in storage.

Regarding the HP operation, its primary operating ranges for Cases C and D are as follows: the evaporator inlet temperature is between 10–40 °C, the condenser outlet temperature is between 45–55 °C, and the modulation is between 30 % and 100 %. Table 5 displays the HP performance within these ranges, demonstrating a higher coefficient of performance when the temperature difference between the evaporator and condenser is smaller and when the HP operates at partial load.

The two case studies illustrate how different load levels influence the HP operation. In Case C, where the load is higher, the HP primarily operates within the modulation range of 65–100 % and an outlet

Test day	1			2			3			4	5	6		
	B0	B1	D	B0	B1	D	B0	B1	D	B0	B0	B0	B1	D
from DG	13	27	60	27	26	35	25	20	23	0	16	8	24	26
from DHN	164	141	114	88	83	75	56	57	45	45	20	112	89	89
Tot	176	168	175	116	109	110	81	77	68	45	37	120	112	115
Ss	7%	16%	28%	24%	24%	30%	31%	26%	31%	0%	45%	7%	21%	19%
Ss,el			35%			32%			34%					23%

Test day	1			2			3			4	5	6		
	B0	B1	D	B0	B1	D	B0	B1	D	B0	B0	B0	B1	D
Not used	12	15	22	8	24	47	21	43	59	14	24	13	19	46
to DHN	32	24	23	62	53	49	244	257	254	50	279	18	9	7
to user	13	27	60	27	26	35	25	20	23	0	16	8	24	26
Tot	57	66	106	97	103	131	290	320	337	64	320	39	52	79
Sc	23%	40%	52%	28%	25%	25%	9%	6%	6%	0%	5%	20%	46%	29%
Uec	79%	77%	76%	92%	77%	63%	93%	87%	82%	78%	92%	66%	63%	39%

Fig. 8. User load sharing between DHN and DG, distribution of DG energy production, and KPIs for the representative days. Case studies B0-B1-D.

Table 5
HP performance within the operating ranges resulting from the test in Cases C and D.

Evaporator inlet temperature [°C]	Condenser outlet temperature [°C]	Modulation	Thermal capacity [kW]	Electricity consumption [kW]	COP
10	45	30 %	2.4	0.53	4.53
10	55	30 %	1.8	0.95	1.92
40	45	30 %	6.5	0.60	10.79
40	55	30 %	5.9	1.03	5.77
10	45	100 %	11.3	3.03	3.73
10	55	100 %	10.7	3.45	3.11
40	45	100 %	15.4	3.10	4.97
40	55	100 %	14.8	3.52	4.21

temperature range of 50–55 °C. In contrast, with a lower load, Case D sees the HP mainly operating at a modulation range of 30–65 % and an outlet temperature range of 53–55 °C. These findings suggest that there is potential for improving the HP efficiency, particularly in Case D. When the HP operates at 55 °C with a modulation below 100 %, it could meet the load requirements at a lower temperature, thereby increasing operational efficiency and enhancing the three KPIs through reduced electricity consumption. Such improvements could be achieved by downsizing the HP and implementing a variable outlet temperature control based on the specific load requirements.

Fig. 7 and Fig. 8 show that in all cases, there is an amount of energy produced by DG and not used that increases moving from A0 to C and from B0 to D. Despite the overall amount increases, the various contributions have a variable trend. Considering the solar circuit preheating, it decreases from Case A0 to C and from Case B0 to D due to the decreasing temperature level of the storage to provide energy to the user due to the strategies implemented. Regarding the thermal losses, they are mainly dependent on the thermal insulation of components (pipes), the thermal efficiency of the HEs and they increase with the increasing of the energy flows: this reflects into the test results where thermal losses increase moving from Case A0 to C and from B0 to D due to the increasing of DG production and energy flow within the substation. Lastly, the energy balance through the storage is the contribution that has the higher increase moving from Case A0 to C and from B0 to D. It is proportional to the difference between the storage temperature at the beginning and end of the day: it includes the storage thermal losses, the amount of energy needed to increase the storage temperature at a level suitable for the load, and the amount of energy that could be potentially used but remains unused. While the first two contributions play a significant role in Cases A0, A1, B0 and B1, the last one is particularly relevant for all the days in Cases C and D thanks to the HP integration that allows a decrease in the minimum useful storage temperature down to 10 °C. At this aim, a potential solution to be explored is a different HP (different size and/or maximum operating temperature) to allow the energy not used to feed into the DHN.

The strategies implemented to enhance self-consumption – including controlling the T_{10} temperature based on climatic conditions, increasing the storage size, and integrating a HP in series with the solar storage – proved effective in both thermal levels of DHN. These strategies not only reduced (or eliminated) grid feed-in on Days 1, 2, and 3, but also increased solar production, making more energy available for self-consumption.

Fig. 7 and Fig. 8 illustrate that a portion of the solar energy is fed into the DHN, even though it could potentially be used to partially or fully meet the user's daily demands (particularly on Days 3, 4, and 5). This is caused by the non-simultaneity between user demand and solar production, as well as by mismatch in terms of power levels; additionally, the values shown were calculated assuming the immediate use of available solar energy from DG. Therefore, further evaluations were conducted under a daily net metering scenario, where the DHN functions as a virtual daily storage system for the energy produced but not immediately self-consumed, allowing it to be reused later in the day. As noted in [47] for Case A0, the energy balance relative to user demand in Cases A1 and C shows a greater contribution from DG: on Day 3, there is a 119 % increase, which allows 100 % self-sufficiency to be achieved, with a share of the solar production fed into the grid as it exceeds user demand. Aside from an insignificant increase on Day 2 (5 % in A1), there are no significant changes on the other days, as solar production is used entirely to meet the user's load, with no feed-in to the grid. In Case A0, this only occurred on Day 6, reflecting the effectiveness of the strategies implemented to increase the share of self-consumption. As expected, the application of net metering has a more pronounced effect in Cases B1 and D, due to the greater compatibility between DHN thermal level, DG production, and user load, particularly on heating days. On Day 3, there are significant increases in the share of DG contributing to load coverage (285 % in B1; 200 % in D), achieving 100 % self-sufficiency with some production fed into the grid. On other days, the increases remain significant, with a DG useful production fully allocated to the user and no feed-in to DHN. This allows B1 and D to reach the following levels of load coverage by DG: from 16-28 % to 30–42 % on Day 1; from 24-30 % to 72–74 % on Day 2; and from 21-19 % to 30–25 % on Day 6.

4.3. Full-year extrapolation

Annual extrapolations for the tested cases and the net metering scenario are shown in the following Fig. 9 and Fig. 10. The tables in these figures also include the relative measurement uncertainty (u_{rel}) as a percentage of the absolute value for each variable considered. It derives from [45] and [47] that detail the measurement uncertainties of the substation installed sensors and how these uncertainties propagate to the derived quantities, such as thermal powers and energies. This paper adopts a similar approach by extending the uncertainty propagation to the KPIs described in Section 3.4. The measurement uncertainty of total production from the DG is assumed to be negligible, as it is an output of the numerical model of the solar field. The variability in the measurement uncertainty of the monitored energy is attributed to differing temperature differences in each HE. In cases of high temperature differences or energy flows, the uncertainty is lower, as seen in HE3 (energy to the DHN), which operates with a temperature difference of 30 °C on the DHN side, or in HE1 (energy from the DHN). Conversely, the uncertainty is higher for HE2 (energy from the DG), which operates at a lower temperature difference and energy flow. Although some KPIs exhibit an uncertainty of up to 10 %, this is still lower than the differences observed among the cases, thereby confirming the validity of the results.

The annual graphs confirm the trends observed in the single-day analysis: self-sufficiency increases from A0 to C, as well as from B0 to D; the user's demands can be supplied by DG via HE2 achieving a S_S of 8 %, 20 %, and 27 % in Cases A0, A1 and C; comparable values can be observed for lower temperature of DHN, with 14 %, 20 %, and 26 % in Cases B0, B1 and D. A share of DG production feeds the DHN (69 %, 54 %, and 45 % in Cases A0, A1, and C respectively), more effectively when the grid operates at lower temperatures (reaching 81 %, 73 %, and 65 % in Cases B0, B1, and D). The implementation of strategies aimed at increasing the share of self-consumption resulted in the following S_C values: 13 %, 28 %, and 30 % in A0, A1, and C; 10 %, 12 %, and 15 % in B0, B1, and D.

By applying the net metering mechanism on a daily basis and extrapolating the results over the entire year, Fig. 9 and Fig. 10 show: an increase in the DG solar energy used to meet the load (up to 38 % in Case C and 58 % in Case D); an increase in self-consumption (39 %, 44 %, and 43 % in A0, A1, and C; 35 %, 34 %, and 33 % in B0, B1, and D), and a corresponding decrease in the share of DG energy fed into the grid (up to −25 % in Cases A0 and B0).

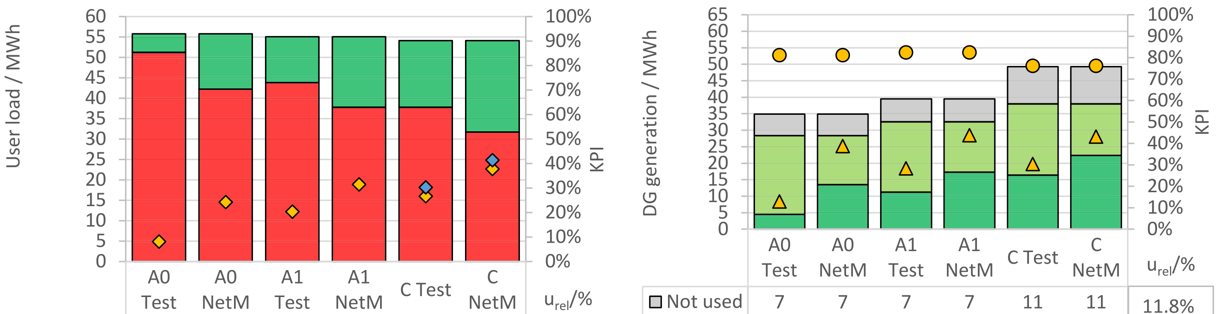

	A0 Test	A0 NetM	A1 Test	A1 NetM	C Test	C NetM	u_{rel}/%
from DG	5	14	11	17	16	22	5.7%
from DHN	51	42	44	38	38	32	3.5%
Tot	56	56	55	55	54	54	3.5%
Ss	8%	24%	20%	31%	27%	38%	9.2%
Ss,el					30%	41%	9.2%

	A0 Test	A0 NetM	A1 Test	A1 NetM	C Test	C NetM	u_{rel}/%
Not used	7	7	7	7	11	11	11.8%
to DHN	24	15	21	15	22	16	0.8%
to user	5	14	11	17	16	22	5.7%
Tot	35	35	39	39	49	49	0%
Sc	13%	39%	28%	44%	30%	43%	5.7%
Uec	81%	81%	82%	82%	76%	76%	2.5%

Fig. 9. User load sharing between DHN and DG, distribution of DG energy production, KPIs and relative measurement uncertainty on an annual basis. Case studies A0-A1-C. Results from experimental test ("Test") and net metering option ("NetM").

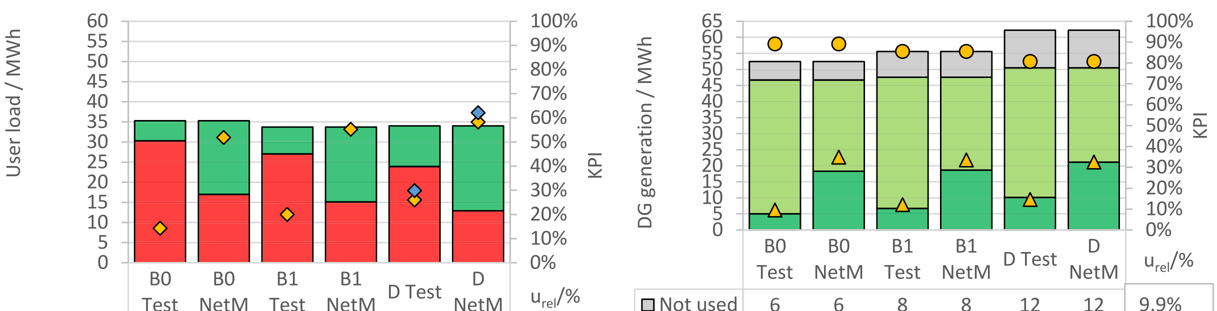

	B0 Test	B0 NetM	B1 Test	B1 NetM	D Test	D NetM	u_{rel}/%
from DG	5	18	7	19	10	21	6.9%
from DHN	30	17	27	15	24	13	3.2%
Tot	35	35	34	34	34	34	3.2%
Ss	14%	52%	20%	55%	26%	58%	10.1%
Ss,el					30%	62%	10.1%

	B0 Test	B0 NetM	B1 Test	B1 NetM	D Test	D NetM	u_{rel}/%
Not used	6	6	8	8	12	12	9.9%
to DHN	42	28	41	29	40	29	0.8%
to user	5	18	7	19	10	21	3.2%
Tot	52	52	56	56	62	62	0%
Sc	10%	35%	12%	34%	15%	33%	6.9%
Uec	89%	89%	86%	86%	81%	81%	1.7%

Fig. 10. User load sharing between DHN and DG, distribution of DG energy production, KPIs and relative measurement uncertainty on an annual basis. Case studies B0-B1-D. Results from experimental test ("Test") and net metering option ("NetM").

5. Conclusions

The paper presents the results obtained from experimental tests on a bidirectional heat exchange substation for district heating, which allows a user to become prosumer, thus giving the possibility to feed into the grid the share of locally produced energy (from renewables or waste heat) and not self-consumed. Based on the results of a previous campaign, described in [47], a series of strategies were implemented to increase the percentage of local production used to supply the user's demands, applying the same methodology (i.e., hardware in the loop and test days) and same boundary conditions for homologous case studies (same load, local generation system, and DHN temperatures). Strategies included managing the discharge temperature of the solar storage and the temperature of energy supply from the substation, controlled according to climate curve (A1-B1); varying the size of the solar storage (A2-B2); and integrating a water-to-water HP in series with the solar storage (C-D).

The data from the annual extrapolation confirm the trends resulting from the analysis of the single test days: the energy produced locally and used to cover the user's demands – described by the self-sufficiency S_S indicator – increases moving from Case A0 to A1, then to C (considering high-temperature grid and a non-renovated building, 8 %, 20 %, and 27 % respectively), and from Case B0 to B1, then to D (considering low-temperature grid and renovated building, 14 %, 20 %, and 26 % respectively). The largest increases occur in the case of non-renovated building and DHN operating at 80 °C-50 °C for supply/return, due to the significant lowering of the temperature for solar energy use in storage compared to the Case A0 configuration. In the net metering scenario, a similar increasing trend can be observed, but with higher percentages: 24 % in A0, 31 % in A1, and 38 % in C; 52 % in B0, 55 % in B1, and 58 % in D. Additionally, there was an increase in solar production (by 15 % and 39 % in A1 and C, respectively, compared to A0, and by 6 % and 18 % in B1 and D, respectively, compared to B0). This was due to a lowering of the utilization temperature of the solar storage, which consequently reduced the average operating temperature of the solar array. As a consequence of the abovementioned effects, the share of DG energy fed into the grid decreases (by 10 % and 24 % in A1 and C, respectively, compared to A0, and by 4 % and 13 % in B1 and D, respectively, compared to B0). Similar effects were observed when comparing the daily energy outputs of Cases A1-A2 and B1-B2 on Day 1, resulting from the increased size of the solar storage.

The implemented strategies have proven effective in increasing the share of self-consumption and enhancing production from renewable sources. Coupling with the net metering mechanism also allows for further exploitation of the local surplus to cover the user's load, even outside the production periods. The presented results could support stakeholders in developing efficient district heating systems, according to the recent EED, particularly in the context of potential thermal energy communities. Future research could focus on the HP, specifically in terms of sizing, maximum operating temperature (high-temperature HP up to 80–90 °C), and temperature management according to load requirements: this would enhance the coupling between solar production, substation, and HP, improving overall performance; additionally, it would enable the feeding of not-used solar energy into the grid at the end of the day and increase the use of the heat pump to meet DHW demands. These benefits could be included into a techno-economic feasibility analysis for the conversion of one or more DHN users into prosumers. This analysis should consider both operational energy costs and capital expenditure, as well as a sensitivity analysis on electricity prices and the fuel costs. Furthermore, the results obtained in this study are highly generalizable and can be applied to other similar contexts, particularly in northern Italy, where district heating networks are predominantly residential and supply space heating and domestic hot water [9]. These findings can thus be effectively transferred to other regions with similar climatic conditions and network configurations, supporting the enhancement of energy production, consumption, and sharing in existing and future district heating systems.

CRediT authorship contribution statement

Paolo Sdringola: Writing – review & editing, Writing – original draft, Project administration, Methodology, Investigation, Conceptualization. **Mauro Pipiciello:** Writing – review & editing, Writing – original draft, Visualization, Software, Methodology, Investigation, Formal analysis, Conceptualization. **Mattia Ricci:** Writing – review & editing, Writing – original draft, Methodology, Conceptualization. **Federico Gianaroli:** Writing – original draft. **Diego Menegon:** Writing – review & editing, Methodology, Investigation, Conceptualization. **Federico Trentin:** Writing – original draft, Software, Investigation. **Francesco Turrin:** Software, Investigation. **Biagio Di Pietra:** Supervision, Methodology.

Declaration of competing interest

The authors declare that they have no known competing financial interests or personal relationships that could have appeared to influence the work reported in this paper.

Acknowledgements

This research was funded in the Program Agreement between the Italian National Agency for New Technologies, Energy and Sustainable Economic Development (ENEA) and the Ministry of Environment and Energy Security (MASE) for the Electric System Research, in the framework of its Implementation Plan for 2022–2024, Project 1.5 “High-efficiency buildings for the energy transition” (CUP I53C22003050001), Work Package 3 “Innovative technologies and components for increasing the energy performance of buildings”.

Appendix

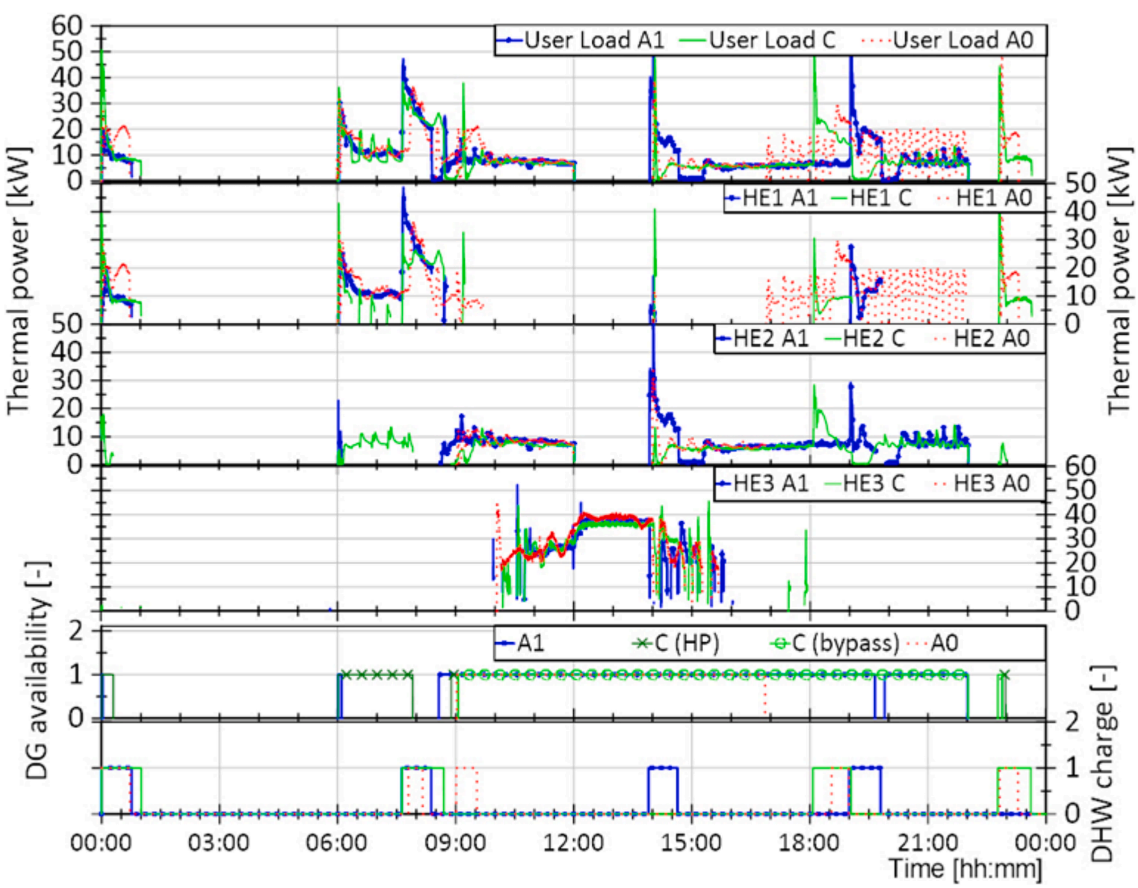

Fig. 11. Day 3. Interaction between the HEs according to thermal demand and DG availability. Case studies A0-A1-C, DHN supply and return 80/50 °C

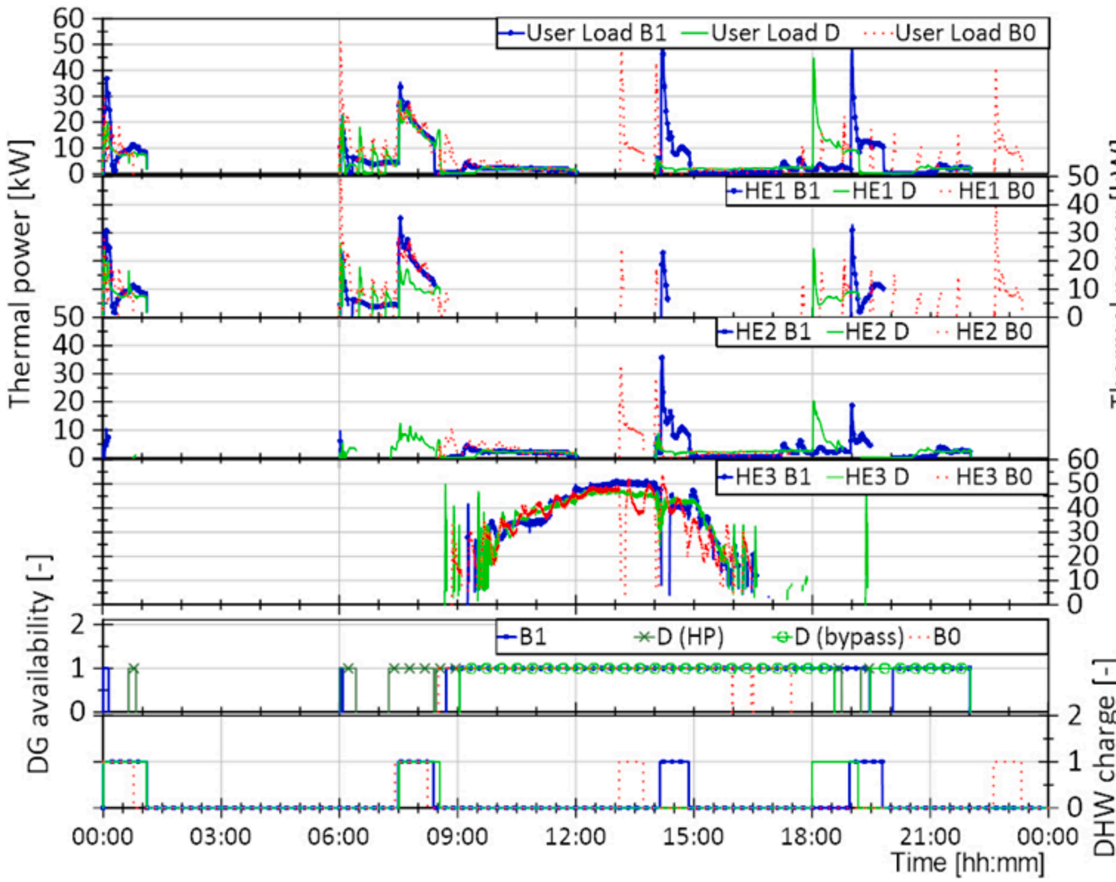

Fig. 12. Day 3. Interaction between the HEs according to thermal demand and DG availability. Case studies B0-B1-D, DHN supply and return 60/30 °C

Data availability

Data will be made available on request.

References

[1] European Climate Law - European Commission Available online: https://climate.ec.europa.eu/eu-action/european-climate-law_en (accessed on 8 July 2024).

[2] K. Difs, National Energy Policies: Obstructing the Reduction of Global CO2 Emissions? An Analysis of Swedish Energy Policies for the District Heating Sector, Energy Policy 38 (2010) 7775–7782, https://doi.org/10.1016/j.enpol.2010.08.037.

[3] A. Billerbeck, B. Breitschopf, S. Preuß, J. Winkler, M. Ragwitz, D. Keles, Perception of District Heating in Europe: A Deep Dive into Influencing Factors and the Role of Regulation, *Energy Policy* 184 (2024) 113860, https://doi.org/10.1016/j.enpol.2023.113860.

[4] Eurostat Available online: https://ec.europa.eu/eurostat/statistics-explained/index.php?title=Renewable_energy_statistics (accessed on 28 March 2023).

[5] V. Bürger, J. Steinbach, L. Kranzl, A. Müller, Third Party Access to District Heating Systems - Challenges for the Practical Implementation, *Energy Policy* 132 (2019) 881–892, https://doi.org/10.1016/j.enpol.2019.06.050.

[6] D. Connolly, H. Lund, B.V. Mathiesen, S. Werner, B. Möller, U. Persson, T. Boermans, D. Trier, P.A. Østergaard, S. Nielsen, Heat Roadmap Europe: Combining District Heating with Heat Savings to Decarbonise the EU Energy System, *Energy Policy* 65 (2014) 475–489, https://doi.org/10.1016/j.enpol.2013.10.035.

[7] District Heating Systems: Uneven Use Around the World Available online: https://www.planete-energies.com/en/media/article/district-heating-systems-uneven-use-around-world (accessed on 25 July 2024).

[8] Energy Efficiency Directive Available online: https://energy.ec.europa.eu/topics/energy-efficiency/energy-efficiency-targets-directive-and-rules/energy-efficiency-directive_en (accessed on 9 July 2024).

[9] AIRU Archives Available online: https://www.airu.it/tag/annuario/ (accessed on 17 February 2025).

[10] E. Bellos, P. Iliadis, C. Papalexis, R. Rotas, N. Nikolopoulos, E. Kosmatopoulos, C. Halmdienst, Dynamic Investigation of Centralized and Decentralized Storage Systems for a District Heating Network, *J. Storage Mater.* 56 (2022) 106072, https://doi.org/10.1016/j.est.2022.106072.

[11] M. Sporleder, M. Rath, M. Ragwitz, Solar Thermal vs. PV with a Heat Pump: A Comparison of Different Charging Technologies for Seasonal Storage Systems in District Heating Networks, *Energy Convers. Manage.: X* 22 (2024) 100564, https://doi.org/10.1016/j.ecmx.2024.100564.

[12] G. Alva, Y. Lin, G. Fang, An Overview of Thermal Energy Storage Systems, *Energy* 144 (2018) 341–378, https://doi.org/10.1016/j.energy.2017.12.037.

[13] A.B. Gallo, J.R. Simões-Moreira, H.K.M. Costa, M.M. Santos, E. Moutinho dos Santos, Energy Storage in the Energy Transition Context: A Technology Review, *Renew. Sustain. Energy Rev.* 65 (2016) 800–822, https://doi.org/10.1016/j.rser.2016.07.028.

[14] A. Buonomano, C. Forzano, A. Palombo, G. Russo, Solar-Assisted District Heating Networks: Development and Experimental Validation of a Novel Simulation Tool for the Energy Optimization, *Energ. Conver. Manage.* 288 (2023) 117133, https://doi.org/10.1016/j.enconman.2023.117133.

[15] D. Čulig-Tokić, G. Krajačić, B. Doračić, B.V. Mathiesen, R. Krklec, J.M. Larsen, Comparative Analysis of the District Heating Systems of Two Towns in Croatia and Denmark, *Energy* 92 (2015) 435–443, https://doi.org/10.1016/j.energy.2015.05.096.

[16] H. Mahon, D. O'Connor, D. Friedrich, B. Hughes, A Review of Thermal Energy Storage Technologies for Seasonal Loops, *Energy* 239 (2022) 122207, https://doi.org/10.1016/j.energy.2021.122207.

[17] T. Yang, W. Liu, G.J. Kramer, Q. Sun, Seasonal Thermal Energy Storage: A Techno-Economic Literature Review, *Renew. Sustain. Energy Rev.* 139 (2021) 110732, https://doi.org/10.1016/j.rser.2021.110732.

[18] D.F. Dominković, B. Ćosić, Z. Bačelić Medić, N. Duić, A Hybrid Optimization Model of Biomass Trigeneration System Combined with Pit Thermal Energy Storage, *Energ. Conver. Manage.* 104 (2015) 90–99, https://doi.org/10.1016/j.enconman.2015.03.056.

[19] J.M. Jebamalai, K. Marlein, J. Laverge, Influence of Centralized and Distributed Thermal Energy Storage on District Heating Network Design, *Energy* 202 (2020) 117689, https://doi.org/10.1016/j.energy.2020.117689.

[20] D. Romanchenko, J. Kensby, M. Odenberger, F. Johnsson, Thermal Energy Storage in District Heating: Centralised Storage *vs.* Storage in Thermal Inertia of Buildings, *Energ. Conver. Manage.* 162 (2018) 26–38, https://doi.org/10.1016/j.enconman.2018.01.068.

[21] G. Manente, A. Lazzaretto, I. Molinari, F. Bronzini, Optimization of the Hydraulic Performance and Integration of a Heat Storage in the Geothermal and Waste-to-Energy District Heating System of Ferrara, *J. Clean. Prod.* 230 (2019) 869–887, https://doi.org/10.1016/j.jclepro.2019.05.146.
[22] M. Turski, R. Sekret, Buildings and a District Heating Network as Thermal Energy Storages in the District Heating System, *Energ. Buildings* 179 (2018) 49–56, https://doi.org/10.1016/j.enbuild.2018.09.015.
[23] M. Mohanraj, L. Karthick, R. Dhivagar, Performance and Economic Analysis of a Heat Pump Water Heater Assisted Regenerative Solar Still Using Latent Heat Storage, *Appl. Therm. Eng.* 196 (2021) 117263, https://doi.org/10.1016/j.applthermaleng.2021.117263.
[24] Y. Song, F. Cao, The Evaluation of the Optimal Medium Temperature in a Space Heating Used Transcritical Air-Source CO2 Heat Pump with an R134a Subcooling Device, *Energ. Conver. Manage.* 166 (2018) 409–423, https://doi.org/10.1016/j.enconman.2018.04.052.
[25] W. Stanek, T. Simla, W. Gazda, Exergetic and Thermo-Ecological Assessment of Heat Pump Supported by Electricity from Renewable Sources, *Renew. Energy* 131 (2019) 404–412, https://doi.org/10.1016/j.renene.2018.07.084.
[26] M. Alhuyi Nazari, J. Rungamornrat, L. Prokop, V. Blazek, S. Misak, M. Al-Bahrani, M.H. Ahmadi, An Updated Review on Integration of Solar Photovoltaic Modules and Heat Pumps towards Decarbonization of Buildings, *Energy Sustain. Dev.* 72 (2023) 230–242, https://doi.org/10.1016/j.esd.2022.12.018.
[27] Z. Meng, Z. Huo, S. Dong, Y. Liu, S. Zhai, C. Ding, K. Hu, J. Yang, W. Han, Simulation Study on the System Performance of Solar-Ground Source Heat Pump Using Return Water of the District Heating Network as Supplementary Heating, *Renew. Energy* 231 (2024), https://doi.org/10.1016/j.renene.2024.120906.
[28] Y. Fan, X. Zhao, Z. Han, J. Li, A. Badiei, Y.G. Akhlaghi, Z. Liu, Scientific and Technological Progress and Future Perspectives of the Solar Assisted Heat Pump (SAHP) System, *Energy* 229 (2021) 120719, https://doi.org/10.1016/j.energy.2021.120719.
[29] Z. Xu, X. Zhang, J. Ji, Research Progress of Phase Change Heat Storage Technology in the Application of Solar Heat Pump, *J. Storage Mater.* 86 (2024) 111272, https://doi.org/10.1016/j.est.2024.111272.
[30] K. Lygnerud, J. Ottosson, J. Kensby, L. Johansson, Business Models Combining Heat Pumps and District Heating in Buildings Generate Cost and Emission Savings, *Energy* 234 (2021) 121202, https://doi.org/10.1016/j.energy.2021.121202.
[31] M. Capone, E. Guelpa, V. Verda, Optimal Installation of Heat Pumps in Large District Heating Networks, *Energies* 16 (2023) 1448, https://doi.org/10.3390/en16031448.
[32] T. Zhu, T. Ommen, W. Meesenburg, J.E. Thorsen, B. Elmegaard, Steady State Behavior of a Booster Heat Pump for Hot Water Supply in Ultra-Low Temperature District Heating Network, *Energy* 237 (2021) 121528, https://doi.org/10.1016/j.energy.2021.121528.
[33] J. Vivian, G. Emmi, A. Zarrella, X. Jobard, D. Pietruschka, M. De Carli, Evaluating the Cost of Heat for End Users in Ultra Low Temperature District Heating Networks with Booster Heat Pumps, *Energy* 153 (2018) 788–800, https://doi.org/10.1016/j.energy.2018.04.081.
[34] T. Reiners, M. Gross, L. Altieri, H.-J. Wagner, V. Bertsch, Heat Pump Efficiency in Fifth Generation Ultra-Low Temperature District Heating Networks Using a Wastewater Heat Source, *Energy* 236 (2021) 121318, https://doi.org/10.1016/j.energy.2021.121318.
[35] T. Zhu, Y. Du, J. Liang, W. Rohlfs, J. Eric Thorsen, B. Elmegaard, Integration of Booster Heat Pumps in Ultra-Low Temperature District Heating Network: Prototype Demonstration and Refrigerant Charge Investigation, *Energ. Buildings* 298 (2023) 113516, https://doi.org/10.1016/j.enbuild.2023.113516.
[36] C. Arpagaus, F. Bless, M. Uhlmann, J. Schiffmann, S.S. Bertsch, High Temperature Heat Pumps: Market Overview, State of the Art, Research Status, Refrigerants, and Application Potentials, *Energy* 152 (2018) 985–1010, https://doi.org/10.1016/j.energy.2018.03.166.
[37] R. Bergamini, J.K. Jensen, B. Elmegaard, Thermodynamic Competitiveness of High Temperature Vapor Compression Heat Pumps for Boiler Substitution, *Energy* 182 (2019) 110–121, https://doi.org/10.1016/j.energy.2019.05.187.
[38] K. Kontu, S. Rinne, S. Junnila, Introducing Modern Heat Pumps to Existing District Heating Systems – Global Lessons from Viable Decarbonizing of District Heating in Finland, *Energy* 166 (2019) 862–870, https://doi.org/10.1016/j.energy.2018.10.077.
[39] C. Mateu-Royo, S. Sawalha, A. Mota-Babiloni, J. Navarro-Esbrí, High Temperature Heat Pump Integration into District Heating Network, *Energ. Conver. Manage.* 210 (2020), https://doi.org/10.1016/j.enconman.2020.112719.
[40] Directive (eu),, *OF THE EUROPEAN PARLIAMENT AND OF THE COUNCIL -. On the Promotion of the Use of Energy from Renewable Sources*, 2018/ 2001.
[41] F. Gianaroli, M. Ricci, P. Sdringola, M. Alessandra Ancona, L. Branchini, F. Melino, Development of Dynamic Sharing Keys: Algorithms Supporting Management of Renewable Energy Community and Collective Self Consumption, *Energ. Buildings* 311 (2024), https://doi.org/10.1016/j.enbuild.2024.114158.
[42] F. Gianaroli, M. Preziosi, M. Ricci, P. Sdringola, M.A. Ancona, F. Melino, Exploring the Academic Landscape of Energy Communities in Europe: A Systematic Literature Review, *J. Clean. Prod.* 451 (2024) 141932, https://doi.org/10.1016/j.jclepro.2024.141932.
[43] A. Dattilo, F. Melino, M. Ricci, P. Sdringola, Optimizing Thermal Energy Sharing in Smart District Heating Networks, Energies 17 (2024), https://doi.org/10.3390/en17122936.
[44] P. Sdringola, M. Ricci, M.A. Ancona, F. Gianaroli, C. Capodaglio, F. Melino, Modelling a Prototype of Bidirectional Substation for District Heating with Thermal Prosumers, *Sustainability* 15 (2023) 4938, https://doi.org/10.3390/su15064938.
[45] M. Pipiciello, M. Caldera, M. Cozzini, M.A. Ancona, F. Melino, B. Di Pietra, Experimental Characterization of a Prototype of Bidirectional Substation for District Heating with Thermal Prosumers, *Energy* 223 (2021) 120036, https://doi.org/10.1016/j.energy.2021.120036.
[46] G.E. Dino, P. Catrini, V. Palomba, A. Frazzica, A. Piacentino, Promoting the Flexibility of Thermal Prosumers Equipped with Heat Pumps to Support Power Grid Management, Sustainability (Switzerland) 15 (2023), https://doi.org/10.3390/su15097494.
[47] M. Pipiciello, F. Trentin, A. Soppelsa, D. Menegon, R. Fedrizzi, M. Ricci, B. Di Pietra, P. Sdringola, The Bidirectional Substation for District Heating Users: Experimental Performance Assessment with Operational Profiles of Prosumer Loads and Distributed Generation, *Energ. Buildings* 305 (2024) 113872, https://doi.org/10.1016/j.enbuild.2023.113872.
[48] T. Testasecca, P. Catrini, M. Beccali, A. Piacentino, Dynamic Simulation of a 4th Generation District Heating Network with the Presence of Prosumers, *Energy Convers. Manage.: X* 20 (2023) 100480, https://doi.org/10.1016/j.ecmx.2023.100480.
[49] T. Rosemann, J. Löser, K. Rühling, A New DH Control Algorithm for a Combined Supply and Feed-In Substation and Testing Through Hardware-In-The-Loop, *Energy Procedia* 116 (2017) 416–425, https://doi.org/10.1016/j.egypro.2017.05.089.
[50] T. Licklederer, D. Zinsmeister, L. Lukas, F. Speer, T. Hamacher, V.S. Perić, Control of Bidirectional Prosumer Substations in Smart Thermal Grids: A Weighted Proportional-Integral Control Approach, *Appl. Energy* 354 (2024), https://doi.org/10.1016/j.apenergy.2023.122239.
[51] Lamaison, N.; Bavière, R.; Cheze, D.; Paulus, C. A Multi-Criteria Analysis of Bidirectional Solar District Heating Substation Architecture. In Proceedings of the Proceedings of SWC2017/SHC2017; International Solar Energy Society: Abu Dhabi, 2017; pp. 1–11.
[52] N. Lamaison, D. Chèze, J.-F. Robin, F. Bruyat, F. Lefrancois, *Operational Behaviour of a Solar-Fed Bidirectional Substation for 4GDH, Networks* (2021) p. 10.
[53] D. Menegon, A. Soppelsa, R. Fedrizzi, Clustering Methodology for Defining a Short Test Sequence for Whole System Testing of Solar and Heat Pump Systems, in: In Proceedings of the Proceedings of SWC2017/SHC2017; International Solar Energy Society: Abu Dhabi, 2017, pp. 1–11.
[54] C. Dipasquale, R. Fedrizzi, A. Bellini, M. Gustafsson, F. Ochs, C. Bales, Database of Energy, Environmental and Economic Indicators of Renovation Packages for European Residential Buildings, *Energ. Buildings* 203 (2019) 109427, https://doi.org/10.1016/j.enbuild.2019.109427.
[55] Jordan, U.; Vajen, K. DHWcalc: PROGRAM TO GENERATE DOMESTIC HOT WATER PROFILES WITH STATISTICAL MEANS FOR USER DEFINED CONDITIONS.; 2005.